DLL Code Tracking of CDMA Signals under Fading and Multiple Access Interference

BY

Hamood-ur-Rehman Khan

A Thesis Presented to the

DEANSHIP OF GRADUATE STUDIES

KING FAHD UNIVERSITY OF PETROLEUM & MINERALS

DHAHRAN, SAUDI ARABIA

In Partial Fulfillment of the
Requirements for the Degree of

MASTER OF SCIENCE

In

Telecommunication Engineering

January 2009

KING FAHD UNIVERSITY OF PERTROLEUM & MINERALS
DHAHRAN 31261, SAUDI ARABIA

DEANSHIP OF GRADUATE SUTDIES

This thesis, written by **Hamood-ur-Rehman Khan** under the direction of his thesis advisor and approved by his thesis committee, has been presented to and accepted by the Dean of Graduate Studies, in partial fulfillment of the requirements for the degree of **MASTER OF SCIENCE** in **TELECOMMUNICATION ENGINEERING.**

THESIS COMMITTEE

Dr. M. Adnan Landolsi (Chairman)

Dr. Ali H. Muqaibel

Dr. Yahya S. Al-Harthi

Dr. Samir H. Abdul-Jauwad
Department Chairman

Dr. Salam A. Zummo
Dean of Graduate Studies

30/5/09
Date

Acknowledgements

esIn the Name of Allah, the Most Gracious, the Most Merciful. All praise and thanks is due to Allah, the Lord of the worlds, who granted me the grace and ability to complete this work. May the peace and blessing of Allah be upon His Prophet Muhammad *salalau alaihim wasalam*.

I gratefully acknowledge the opportunity and support provided to me by the King Fahd University of Petroleum & Minerals to complete this research.

With a deep sense of appreciation, I would like to express my sincere gratitude to my thesis advisor, Dr. Mohammed Adnan Al-Andalusi, for his guidance, help and patience in supervising this work and in motivating me whenever I encountered obstacles. I would also like to thank my learned committee members, Dr. Ali Hussain Muqaibel and Dr. Yahya S. Al-Harthi, for their meticulous reviews and comments on my research.

I would like to thank my friend and colleague, Mohammad Abdul Lateef, for translating the abstract into Arabic despite his tight schedule and I wish him well in all his future endeavors.

I offer sincere thanks to my parents, sisters and brothers for their love, guidance and support in everything I ever did. Special thanks go to my father for his unwavering support and understanding during my research. May Allah take excellent care of my family and bestow His mercy on them.

Table of Contents

List of Figures

ABSTRACT

Name: Hamood-ur-Rehman Khan

Title: DLL Code Tracking of CDMA Signals under Fading and Multiple Access Interference

Degree: Master of Science

Major Field: Telecommunication Engineering

Date: January, 2009

In CDMA systems fine synchronization of the incoming and local spread-spectrum signals is crucial for overall system performance. The Delay Lock Loop (DLL) has been traditionally used to achieve this. In the present study two different DLL architectures are considered: the non-coherent DLL and the RAKE-like combining DLL. An extensive study of DLL performance using analytical techniques is undertaken. The analysis takes into account realistic channel conditions such as multipath fading and multiple access interference. Quadrature phase spreading is considered in accordance with current 3G/UMTS standards. The statistics for the residual tracking error are obtained for various channel conditions such as low and high SNRs, Rayleigh and Rician fading models, and for various levels of multiple user interference. Finally, the analysis is applied to positioning scenarios in a cellular network, where the accuracy of the signal time-of-arrival (ToA) measurements between the Mobile and Base Stations plays a fundamental role.

Keywords: CDMA, delay lock loop, code tracking, QPSK, Rayleigh fading, Rician fading, time-of-arrival measurements, wireless positioning, multipath interference, multiple access interference, RAKE-combining.

ملخص الرسالة

الإسم: حمود الرحمن خان.

عنوان الرسالة: تتبع شفرات DLL لإشارات CDMA مع تلاشي الإرسال و التداخل متعد الوصول.

الدرجة: الماجستير في هندسة الاتصالات.

التاريخ: يناير – 2009م

يعتبر التزامن بين الرسالة النستقبلة و المحلية أمر مهم في مجمل أداء أنظمة CDMA. و جرت العادة على إستخدام DLLلتحقيق هذا التزامن.في هذا العمل تستخدم تصميمين مختلفين لـDLL: DLL غير متزامنة و DLL شبيهة بتجميع RAKE. لقد تمت في هذا العمل دراسة مكثفة لأداء DLL باستخدام الطرق التحليلية. اطرق التحليلية المستخدمة تأخذ في الاعتبار حالات واقعية لقناة الإرسال مثل التلاشي متعدد الإتجاهات و التداخل متعدد الوصول. يستخدم في هذا العمل التوسيع الزاوي الرباعي طبقا للمعايير المستخدمة حاليا في أنظمة 3G/UMTS. يتم الحصول على الإحصاءات لتتبع ما تبقى من خطأ في أوضاع مختلفة لقناة الإرسال ، مثل علو أو إنخفاض SNR ، نماذج تلاشي Ricean و Rayleigh ، بالإضافة إلى مستويات مختلفة من التداخل متعدد الوصول. و أخيرا تم تطبيق التحليلات علي سيناريوهات تحديد الموقع في الشبكة الخلوية ، حيث تؤدي دقة إشارة وقت الوصول (ToA) بين قياسات الجوال ومحطات القاعدة دورا أساسيا.

الكلمات الرئيسية: CDMA ، التزامن، حلقة قفل التأخير، تتابع الشفرات، تلاشي Rayleigh، تلاشي Ricean، قياسات زمن الوصول، تحديد المواقع اللاسلكي، التداخل متعدد الإتجاهات، التداخل من باقي المستخدمين، تجميع RAKE.

Chapter 1 Introduction

1.1 Overview of CDMA Systems

Code Division Multiple Access (CDMA) is a multiple access technique used to share a single communication channel among several users. The sharing of the channel is done to maximize capacity by allocating the available bandwidth to multiple users without severely degrading the system performance. CDMA is one of the three major techniques used to share bandwidth in a communication system, the other two being Frequency Division Multiple Access (FDMA) and Time Division Multiple Access (TDMA) [1].

In FDMA the available spectrum is divided into different frequencies and assigned to different users. At any given time, multiple users access the channel using the frequencies assigned to them. In TDMA the communication channel is split into time slots, allowing each user to access the entire channel for a short duration of time. Other users access the channel at the same frequency during a different time slot. If a channel time slot is not used, it sits idle and cannot be used to increase the spectral efficiency of the system.

CDMA, however, is based on spread spectrum technology. All users occupy the communication channel simultaneously. Transmission is spread over the entire radio band, and each call is assigned a unique "spreading" code to differentiate it from other calls carried over the same frequency. Transmission occurs independently and asynchronously. The power transmitted by each user is controlled to give the signal-to-noise ratio required for a given performance level. In this

way the system does not attempt to allocate disjoint frequency or time resources to each user, but instead all resources are allocated to all users simultaneously. Each user's "spreading" code is used to generate a noise-like wideband signal occupying the entire frequency allocation for as long as it is needed. These spreading sequences (or codes) are binary, and they have desirable autocorrelation and cross correlation properties, which include very low autocorrelation values for nonzero offsets and noise-like cross correlation values. Each user thus contributes to the background noise affecting all users, but to the least extent possible. The additional interference limits capacity, but, because time and bandwidth resource allocations are unrestricted, the resulting capacity is significantly greater than for conventional systems [2].

1.2 Synchronization in CDMA Systems

Spread spectrum systems employ the same basic elements of a conventional digital communication system. Conventional digital communication systems require carrier synchronization to take care of frequency and phase differences between the received signal and the signal that is expected at the receiver. In addition to this, spread spectrum systems require synchronization of the spreading code. Code synchronization is used to synchronize in time the code received from the transmitter with the code generated at the receiver. Figure 1-1 shows a generic spread spectrum system with the PN sequence generator at the transmitter and the receiver.

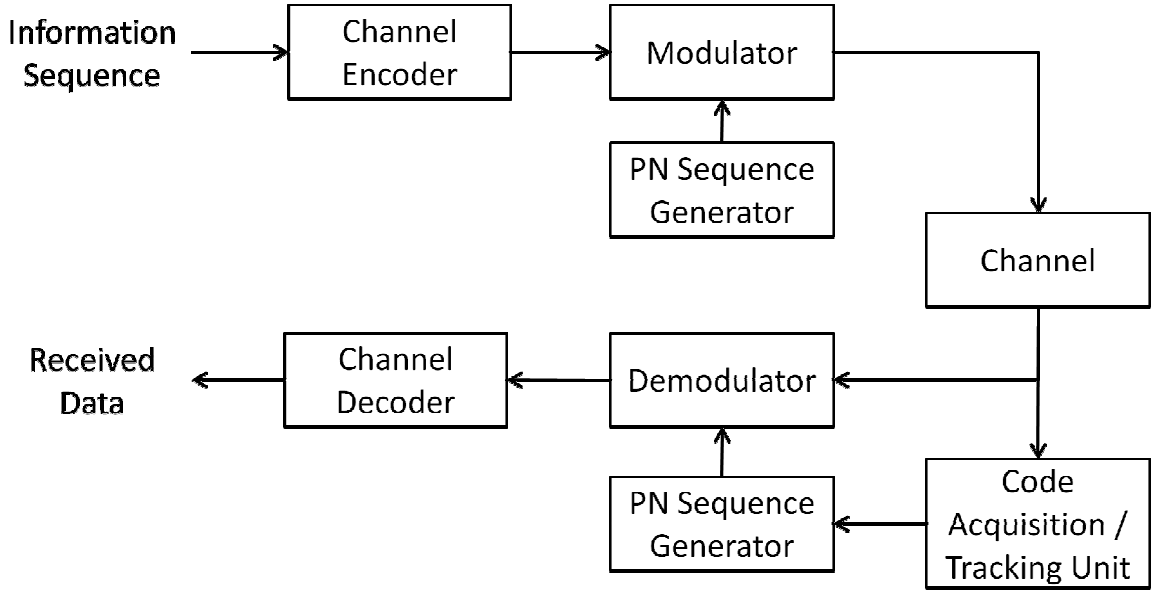

Figure 1-1: A simplified block diagram of a spread spectrum system

Synchronization of the PN sequences generated at the receiver with the PN sequences contained in the received signal is required in order to properly despread the received spread spectrum signal. At the receiver, therefore, the carrier phase, frequency and code timing have to be properly synchronized to the received signal for accurate detection of the transmitted information. In a practical system, synchronization is established prior to the transmission of the information by transmitting a fixed PN bit pattern which is designed so that the receiver will detect it with high probability in the presence of interference [3]. After time synchronization of the PN sequence is established, the transmission of information starts.

The efficiency of a spread spectrum system is highly dependent on the capability of the receiver to continuously maintain this synchronization between the received signal PN code and the locally generated PN codes. Several analyses have been made on the performance of CDMA systems with the assumption that there is perfect PN synchronization. However, PN synchronization is one of the most difficult tasks in spread spectrum communication systems. Synchronization of the receiver to

the received spread spectrum signal is separated into two distinct phases: code acquisition and code tracking.

1.2.1 Code Acquisition

During acquisition, the receiver obtains the relative delay between the received signal and the locally generated code to within a code chip interval. The normalized delay between the input and local sequence is made less than one, where the normalization constant is the chip symbol duration. The usual procedure for establishing initial synchronization is for the transmitter to send known pseudo-noise data sequence to the receiver [3]. The receiver is continuously in search for this known sequence in order to establish initial synchronization. There is no prior knowledge of the received signal, and hence the sequence must be searched by testing different phases of the internal sequence against the received signal. The matched filter or cross correlation are the optimum methods for estimating delay and for establishing initial synchronization. A filter matched to the known data waveform generated from the known pseudorandom sequence continuously looks to exceed a predetermined threshold.

When this threshold is exceeded, initial synchronization is established and the demodulator starts the tracking mode. Alternatively, a sliding correlator may be used. The correlator cycles through time uncertainty, usually in discrete time intervals of half a chip interval, and it correlates the received signal with the known synchronization sequence. Cross correlation is performed over the whole time interval. The correlator output is compared with a threshold to determine whether the known signal sequence is present. If the threshold is not exceeded, the known reference signal is advanced in time by half a chip interval and the correlation process is repeated. These operations are performed until a signal is detected or until the search has been performed over the whole time uncertainty interval [2].

There are different approaches to these operations, with different acquisition times and complexities. The least complex, but the slowest, is the completely serial algorithm which tests each phase of the internal sequence against the received signal. The most costly and complex, though also fastest, is the completely parallel algorithm where different phases of the sequence are compared simultaneously. In practice, however, total parallelism is out of the question when the sequence is very long and simpler solutions are necessary. Between these two extreme solutions there are a variety of hybrids using different degrees of parallelism.

1.2.2 Code Tracking

Further adjustment, to remove the slight maladjustment left and to fine-tune the delay as close to zero as possible is done during tracking. The development of closed loop techniques for accurate PN tracking plays an important role in supporting the acquisition process once the code has been acquired. The optimum design and true assessment of the performance of the PN tracking loop is an essential component of the overall receiver design [4]. If the received signal is out of synchronism by a fraction of a chip, insufficient signal energy will reach the demodulator, resulting in inaccurate detection of the transmitted information. The tracking process is the focus of this work.

Code tracking is accomplished by using phase-locked techniques similar to those utilized for carrier tracking. The principal difference between the phase-locked loop techniques used for carrier tracking and those used in code tracking is the implementation of the phase discriminator [5]. Unlike the implementation of the phase discriminator in code tracking, traditional phase-locked loop techniques employ several multipliers, pairs of filters and envelop detectors. The phase discriminator utilized in code tracking makes use of correlation operations between the received signal and the two different phases, early and late, of the receiver generated spreading waveform. A

tracking loop that makes use of the independent correlators is called a delay-lock tracking loop (DLL) [6], [7], [8], [9]. The DLL can be operated in a coherent or noncoherent mode, depending on the system application [4]. Coherent loops make use of the received carrier phase information while noncoherent loops do not. The delay lock loops use what is called the early-late gate structure [7]. It maintains synchronization of the receiver's replica of the spreading code by using two correlators called an early correlator and a late correlator. An early correlator uses a code reference waveform that is advanced in time by some fraction of a chip with respect to the currently estimated code phase. A late correlator uses a code reference waveform that is delayed by some fraction of a chip. The difference between the early and late correlations is used to sense small deviations of the incoming spreading code's timing with respect to the early and late code timing. If the synchronization is not exact, the filtered output from one correlator will exceed the other, and a voltage controlled oscillator (VCO) will be appropriately advanced or delayed. The VCO is a clock in the sense that it drives the PN code generator so that, when the PN code generator clock is lagging in phase in comparison with the incoming sequence phase, it drives the clock faster, and vice versa. At equilibrium point, the two filtered correlator outputs will be equally displaced from the peak value and the PN code generator output will be exactly synchronized to the received signal that is fed to the demodulator [2]. Once the sequence timing is acquired and tracked accurately, the spreading can be removed by multiplying the incoming signal with the replica of the PN sequence used at the transmitter to spread it.

1.3 Wireless Positioning in CDMA Networks

Wireless position location has received considerable attention over the past decade. Position location using radio signals has been used by the military for years (e.g. the GPS). It is a relatively recent application in civilian radio systems. The military has expended great effort to build a highly

accurate location system for its various branches, but civilian industry has a more difficult time justifying the tremendous cost of developing such a system. Consequently, intensive research has been done on location methods which utilize the existing and future wireless system components, i.e. base stations (BSs) and mobile stations (MSs).

In a CDMA system, radiolocation can be implemented on the forward link or the reverse link. With forward link location, the MS uses signals transmitted by several BSs to calculate its own position (self-positioning). This is the approach used in GPS where satellites are used instead of terrestrial BSs. With reverse link location, several BSs measure the signals transmitted by the MS and relay them to a central site for processing (remote-positioning). For location in CDMA networks, the second approach has the advantage of not requiring and modifications or specialized equipment in the MS handset, thus accommodating the large pool of handsets already in use in existing cellular networks.

There are three primary methods of positioning: those based on signal strength measurements (SoA), angle of arrival (AoA) or time of arrival (ToA) measurements [10], [11], [12], [13], [14], [15], [16], [17]. The signal measurements are first used to determine the length or direction of the radio paths to/from a MS from/to multiple BSs, and then known geometric relationships are used to determine the location [15]. Hybrid methods involving more than one of these methods simultaneously are also possible and have been studied. In general, locating a MS in two dimensions requires a minimum of three sets of measurements from corresponding BSs, though two BSs could suffice in AoA methods. Multiple BSs are needed in order to resolve the ambiguities arising from multiple crossings of the lines of position. The lines of positions are the curves that describe the possible location of the MS with respect to a single BS for each of the signal strength, AoA, and ToA methods. For time difference of arrival (TDoA) methods, lines of positions are defined with respect to two BSs. Each of the lines of position can be described

mathematically with respect to the relative geometry of the BS and MS. Figure 1-2 shows a mobile positioning scenario where two BS are co-locating a MS using ToA measurements.

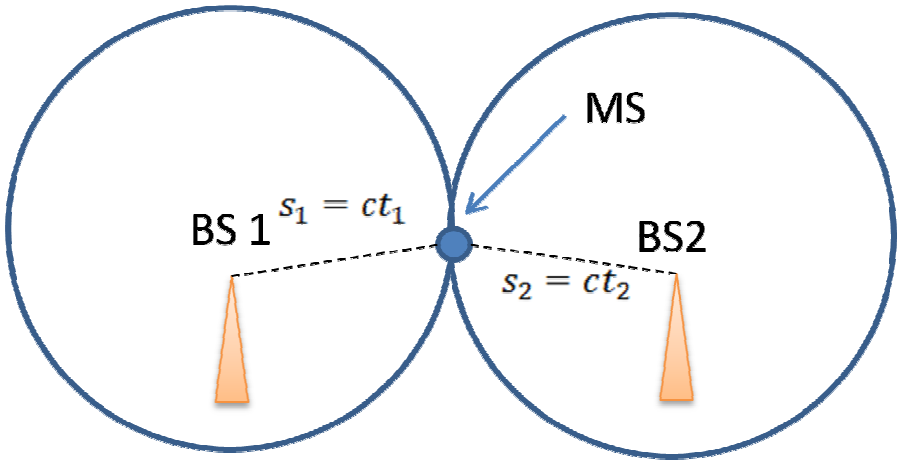

Figure 1-2: Mobile positioning scenario where two BS co-locate a single MS using ToA measurements

The conventional methods of code tracking for CDMA signals (e.g. DLLs) can be used directly to take measurements of time delays for ToA based positioning. Any analysis related to the DLL's performance or modification of the basic DLL has direct implications for the performance of the radiolocation algorithm that will process these measurements. So the traditional DLL loop in CDMA systems takes an added significance as the primary mechanism for carrying out time delay estimation. This factor is a strong motivation for carrying out the proposed investigation of code tracking loops in the present thesis.

1.3.1 Sources of Error in DLL Code Tracking and ToA Estimation

Error can be introduced in the time tracking estimates of the DLL through various means. Accuracy of the code tracking process depends on the exact implementation of the DLL. Aside from implementation details, the operating environment plays a key role in DLL performance. Following [18], we will assume that limitations imposed by hardware are negligible. These include quantization effects, the precision of the DSP hardware or signal distortions introduced by the RF frontend. We will focus on errors that result from the medium through which signals pass before they are measured by BS equipment. Such sources of error in wireless communication systems include multipath propagation, multiple access interference (MAI) and non-line-of-sight propagation [15], [19], [20]. Non-line-of-sight (NLoS) propagation describes the scenario where the direct or Line-of-Sight LoS path between the MS and BS is blocked by some structure (e.g., buildings, mountains). For CDMA, interference from other users contributes to the error [21]. This interference is known as multiple access interference or MAI. In the present study we will deal exclusively with multipath and multiple access interference.

Multipath propagation is described by the reception of multiple signals at a MS or BS. These signals can combine constructively (large signals) or destructively (smaller signals) and they result in the phenomenon known as *fading*. The multiple signals that are received make it difficult to accurately determine the signal ToAs. Path loss models are difficult to use because of the high variability of the received signal strength in mobile radio systems. Fading caused by multipath can be either flat or frequency selective. In flat fading, delay spread of the channels is smaller than the chip duration, but in frequency selective fading the reverse is true. We will use appropriate models for both flat and frequency selective fading in our analysis.

All cellular systems suffer from co-channel interference. In CDMA, users share the same frequency band with different spreading codes. Hence, their reverse link transmissions interfere with one another, resulting in the near-far effect and making it difficult to recover the weaker users [22], [23]. The near-far effect can be described as follows. Consider a receiver and two transmitters, one close to the receiver, the other far away. If both transmitters transmit simultaneously and at equal powers, then due to the inverse square law the receiver will receive more power from the nearer transmitter. Since one transmission's signal is the other's noise, the signal-to-noise ratio (SNR) for the farther transmitter is much lower. This makes the farther transmitter more difficult, if not impossible, to detect. If the nearer transmitter transmits a signal that is orders of magnitude higher than the farther transmitter, then the SNR for the farther transmitter may be below detectability. This effectively jams the communication channel. In short, the near-far problem is one of detecting or filtering out a weaker signal amongst stronger signals.

Power control schemes, which attempt to ensure that each user's signal is received with equal power at the BS, [22], [23], can be used to combat the near-far effect. But for CDMA cellular systems, the near-far effect remains a factor even when power control schemes are used since the interference will affect the ability of a conventional receiver at other BSs to synchronize/estimate the ToA information. The effects of MAI on code tracking techniques, such as the conventional DLL, have been shown to be quite drastic [18].

1.4 Thesis Motivation

CDMA is an important area in the field of communications research because of its increased system capacity and improved spectral efficiency. Wireless positioning in CDMA networks is another area of active research and development, because of its value for safety and security

applications as well as commercial uses. Functions related to both of these areas (communication and wireless positioning) rely crucially on the performance of the code tracking subsystem in the CDMA receiver at either the MS or the BS. Different approaches have been developed for estimation of time-of-arrival from the received signals. These methods include coarse code acquisition [24], [25], code tracking using delay lock loops-DLL [19], as well as other methods based on Fourier techniques [26], subspace-based code acquisition [27], and Kalman filter based code tracking. Since the focus of this work is on practical scenarios for mobile positioning CDMA networks, we consider the most commonly adopted method of ToA estimation of propagation delays using spread spectrum signaling—namely, code tracking loops, or DLLs. The DLL-based approach provides good accuracy without entailing additional costly signal processing requirements. The statistics of the code tracking error are directly needed to evaluate the performance of location algorithms that employ ToA measurements.

1.5 Thesis Contribution

The most widely used performance measure for the DLL is the variance (or equivalently the standard deviation) of the residual timing error. The variance of this timing error is a function of the SNR in the loop bandwidth. However, for the purpose of mobile positioning, we are more interested in deriving the full statistics (probability density function-PDF) of the timing estimation error, and this is the focus of the present study.

The primary contribution of this thesis is the performance analysis of the traditional non-coherent DLL and the RAKE-like combining DLL under realistic channel conditions, where RF cellular propagation, multipath fading, and multiple access interference are taken into account. The statistics for the residual tracking error are obtained by analytical derivations for various scenarios

of interest. As noted before, these statistics are essential to network-based mobile positioning, where the accuracy of the ToA estimates between the mobile and base stations plays a fundamental role.

In most previous research, ToA location algorithms typically assumed that the time of arrival measurements are Gaussian-distributed, with a given variance (or standard deviation) value. Although at high SNR this approximation seem plausible, this no longer holds true at low SNR (e.g., for the case of MS signal reception at a far away, non-serving BS), as our results show. Furthermore, there is a qualitative difference between the error PDFs obtained under Rician and Rayleigh fading conditions. Rician fading model is a more appropriate model for LOS propagation, while the Rayleigh model is applicable for NLOS conditions (where there is no specular component, only diffuse components). It should be pointed out that in previous research, when making the Gaussian assumption, the variance of the ToA timing measurements was sometimes assigned rather arbitrarily, with no obvious relationship to other system parameters. Even where system parameters were taken into account, the tracking error variance was obtained by using an approximate linearized model for the DLL, which only holds true in the case of high SNRs.

In our study, we model the residual error process more accurately by analyzing the full non-linear model for the DLL and we address system issues that affect DLL performance (such as number of users, specific cellular topology, level of MS handoff connectivity, etc). The probability distributions that we compute are obtained analytically rather than through simulations. This enables the performance evaluation to be extended to a wide range of system parameters. Specifically, we give a comprehensive analytical framework for obtaining the DLL ToA error statistics under all different combinations of system conditions, for low and high SNRs, Rayleigh and Rician fading models, and for various levels of multiple user interference. We also extend the previous analysis with respect to the modulation being used. In previous research, BPSK

modulation and spreading was assumed. In our present work we consider quadrature phase modulation and spreading in view of the current 3G UMTS standard.

1.6 Previous Work

In several papers the delay lock loop (DLL) was analyzed. The earliest work on code tracking discriminators was done by Spilker and Magill [6] where it was shown that the proper error signal for tracking could be derived from a correlation of the received signal with a receiver generated first derivative of the spreading waveform. Later work by Spilker [7] discussed the theory of operation and evaluation of the performance of a DLL in the presence of additive white Gaussian noise. The work by Gill [8] extended this work and derived the tracking performance for the coherent and non-coherent implementations. Hartmann [28] analyzed the performance for a non-coherent loop in the presence of white Gaussian noise and based his analysis on variance and code delay error. An envelope detector (noncoherent) was used. The signal-to-noise performance of the square-law loop is approximately 3dB worse because of non-coherent squaring loss. The results were derived under the assumption of additive white Gaussian noise at the input of the loop. Meyr ([29], [30], [31]) was the first to introduce the idea of modeling the stochastic time evolution of the phase error in a tracking loop as a renewal Markov process. Unlike carrier tracking loops where the nonlinear phase error characteristic is periodic, code tracking loops have an essentially aperiodic phase error characteristic. The characteristic is of finite range. When the code tracking loop loses lock, the error process is bound to reach a finite boundary within a finite time. Code tracking loops can therefore be modeled using the renewal theory approach. Polydoros and Weber [32] applied this renewal theory to the study of the aperiodic finite phase error characteristic for the case of a noncoherent delay lock loop. The exact renewal theory approach was compared to the approximate periodic extension approach and it was found that for low signal-to-noise ratio (SNR), the exact

and approximate theories could deviate while at high SNR they yielded identical performance. Simon [9] performed the optimum design and performance of the noncoherent DLL configuration, investigating the band limiting effect of the bandpass arm filters and demonstrating that for some fixed data rate and SNR, there exists an optimum filter bandwidth in the sense of minimizing the loops tracking jitter. Coherent loops were discussed in [7], [8] while the more practical Noncoherent loops were discussed in [9], [28] and [33]. Noncoherent loops are important because they are insensitive to data modulation and do not presume reliable carrier tracking prior to code acquisition as do coherent loops [34]. The performance analysis of the conventional noncoherent DLL (NCDLL) for additive white Gaussian noise channels was done in [32].

Work has been done to enhance the performance of the DLL by modifying the DLL structure. A modified noncoherent DLL was first introduced by Yost and Boyd [38]. Instead of using the early and late gate structure to form the error the signal, the difference between the early and late signals was *mixed* with the received signal to form the error signal. The loop was shown to have a superior tracking performance to the traditional DLL. The authors further considered the band-limiting effects of the bandpass arm filters on the performance of the modified DLL demonstrating its increased performance below a certain SNR. Further improvement on the work by Yost and Boyd was done by [35] where the proposed design increases the number of correlations by addition of two new phase shifted PN reference signals, advanced and delayed by a period, thus allowing the loop discriminator characteristics to be shaped in such a way so as to expand the loop's correlation range without affecting the lock-in range.

The DLL performance can suffer severe degradation under fading and multiple access interference. Recent research investigated the effects of these performance mitigating factors. Prominent among these were [36], [37], [38], and [39]. In [36] the probability distribution of the residual tracking error was computed numerically under flat fading Rayleigh and Log-normal fading conditions. In

[39] a frequency selective, slow-fading, multipath channel with uncorrelated scattering was considered. The study in [39] also considered the performance degradation due to multipath errors. In [37] the effects of multiple access interference (MAI) on the DLL performance were analyzed under AWGN channel by using the Fokker-Plank method of [29]. Modified code tracking loops have been developed that give improved performance in multipath channels, as in [40], [41], [42] and [43].

1.7 Organization of the Thesis

The thesis is organized as follows:

- Chapter 2 presents an analytical result for the case of a RAKE-like combining DLL considered in [44]. We extend the analysis presented three respects. First we consider quadrature spreading. Second, we incorporate Rician fading channels to model Line-of-Sight (LOS) signal propagation. Thirdly, we describe the full tracking error probabilities instead of just giving the error variance.

- Chapter 3 presents the analysis of a non-coherent DLL operating in a Rayleigh/Rician frequency selective fading channel. Again, a quadrature phase spreading is considered and full first order tracking error probabilities are presented for different scenarios.
- Chapter 4 considers how the analysis of chapter 2 and 3 can be applied to mobile positioning in a typical cellular network environment for various scenarios of MS and BS configurations.
- Chapter 5 concludes with a summary and a discussion for possible future work.
- Appendix A gives the derivation and solution of the one dimensional Fokker-Plank equation employed in the analysis of Chapter 2.

- Appendix B gives the derivation of the autocorrelation function of the total noise used in the DLL model of Chapter 2.

Chapter 2

Code Tracking using the RAKE-combining DLL

As discussed in Chapter 1, spread-spectrum communication requires that the transmitter and receiver spreading waveforms be synchronized. If the two waveforms are out of synchronization by as little as one chip, insufficient signal energy will reach the receiver data modulator for reliable data detection. The task of achieving and maintaining code synchronization is always delegated to the receiver. Code synchronization is achieved by the acquisition unit, which synchronizes the incoming spreading code with the locally generated code at the receiver to within a chip period, where the chip period is defined as the duration of the code symbol in the spread waveform. Once coarse synchronization has been achieved, the code tracking loop takes over to obtain and maintain precise code synchronization between the transmitter and the receiver.

Code tracking loops can be categorized as either coherent or noncoherent. Coherent loops make use of the received carrier phase information, whereas noncoherent loops do not. In this chapter a modification of the traditional coherent delay lock loop is considered. The modified structure is based on the work in [44]. An analysis of this modified DLL for signals over multipath frequency-selective fading channels is presented. CDMA signaling schemes with quadrature-spreading are considered on the basis of 3G UMTS standard, and a multi-DLL structure is used for individual tracking and maximum-ratio combining of the resolvable multipath signals. The residual timing error statistics are derived analytically by using the Fokker-Plank method [45]. It is shown that the maximum-ratio combining (RAKE-like) approach can exploit the diversity of the channel to

greatly enhance the tracking performance of the DLL (similar to the gain achieved with MRC in data detection). The channel gain and phase estimates are required because the DLL is coherent. Following [44], it is assumed that perfect channel estimates of the channel impulse response are available at the receiver. Numerical results and comparisons with the conventional coherent DLL show that the proposed scheme can reduce the residual error tracking variance by more than an order of magnitude over a wide range of received SNR values.

This chapter is organized as follows. We first consider the overall system model for the coherent-combining DLL. The model takes into account quadrature spreading and multipath fading. A two-path Rician/Rayleigh fading channel is considered. Secondly, we develop the Stochastic Differential Equation that describes the dynamic behavior of the loop. It governs how the tracking error changes with time. The tracking error statistics are then seen to satisfy a Fokker-Plank equation under reasonable assumptions. The associated Fokker-Plank is then solved to obtain the steady-state tracking error probability distribution. To solve the Fokker-Plank equation, the autocorrelation function of the total noise at the input of the DLL is needed. This autocorrelation function of the total noise is derived first. The tracking error statistics are then computed by using a four-dimensional Monte Carlo integration. Finally, the tracking error statistics for a conventional, non-combining DLL under multipath fading are compared with those of the combining DLL that is under investigation.

2.1 System Model

The system that we employ was developed in [44] for BPSK spreading. We extend the model to incorporate QPSK spreading as in the current 3G/UMTS standards. We consider a T_C-spaced tapped delay line model for the multipath channel, where T_C is the chip duration of the spreading

code. An unmodulated pilot sequence is transmitted for code tracking. Figure 2-1 depicts direct sequence (DS) spread spectrum signaling on a multipath channel. Here $c_I(t)$ is the in-phase and $c_Q(t)$ is the quadrature phase spreading function, and ω_C and P are respectively the radian frequency and power of the carrier, and $g(t,\tau)$ is the channel impulse response at time t and delay τ. The I and Q spreading functions are taken to be orthogonal m-sequences with a root-raised cosine chip shaping function having a roll-off factor of 22%.

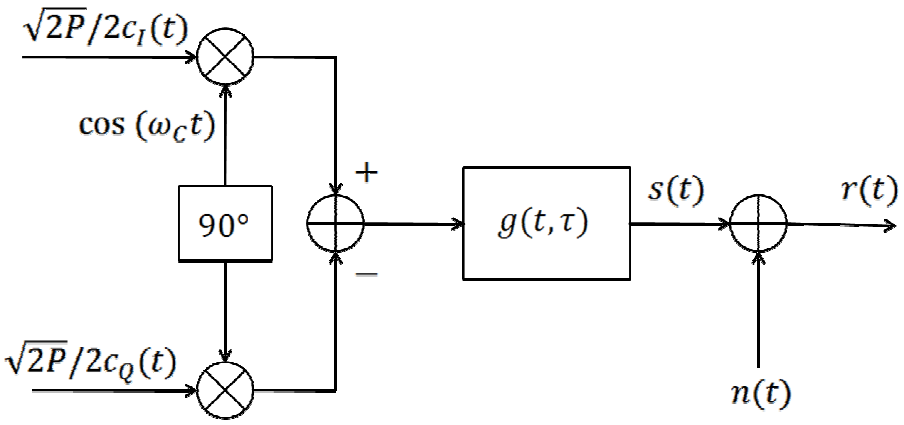

Figure 2-1: Direct-sequence spread spectrum signaling on a multipath fading channel

Let $\tau(t)$ denote the channel time-delay and $c(t) = c_I(t) + jc_Q(t)$ be the complex envelope of the quadrature spreading waveform. Since $\tau(t)$ is the time delay of the channel, $g(t,\zeta) = 0$ for $\zeta \leq \tau(t)$. Assuming that the multipath intensity profile has L paths, it will be zero outside the delay interval $[\tau(t), \tau(t) + (L+1)T_C]$. The complex envelope of the noiseless signal $\mathrm{s}(t)$ in Figure 2-1 can be represented as

$$\tilde{s}(t) = \sum_{k=0}^{L} c(t - \tau(t) - kT_C)g_k(t) \tag{2.1}$$

From 2.1 the channel can be modeled by the T_C-spaced tapped delay line shown in Figure 2-2. The complex tap gains $g_k(t) = g_{ck}(t) + jg_{sk}(t) = a_k(t)e^{j\theta_k(t)}$ are Gaussian random variables, where

$$a_k(t) = \sqrt{\left(\ g_{ck}(t)\right)^2 + \left(g_{sk}(t)\right)^2} \tag{2.2}$$

and

$$\theta_k(t) = \text{Tan}^{-1}\frac{g_{sk}(t)}{g_{ck}(t)} \tag{2.3}$$

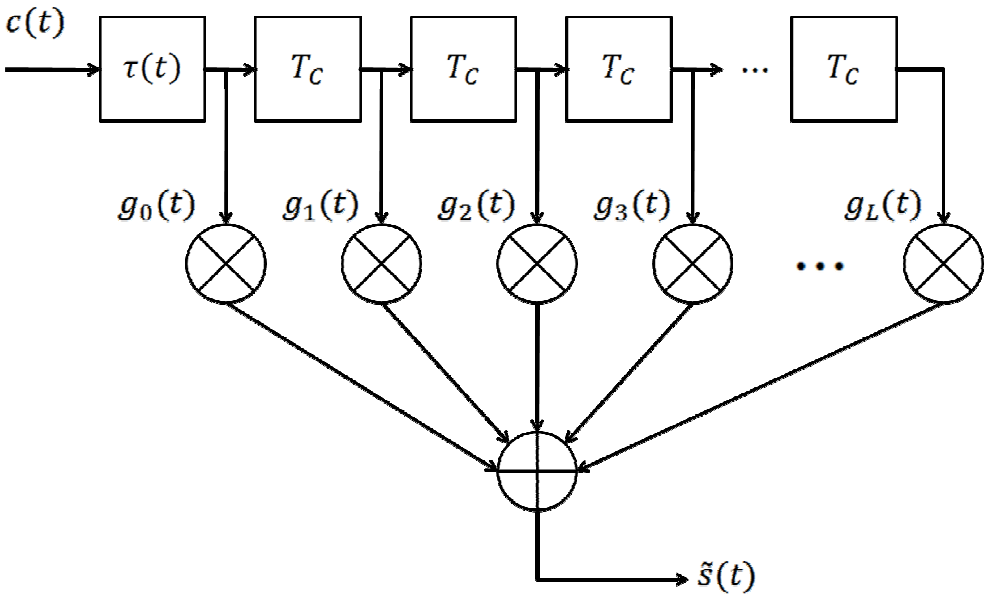

Figure 2-2: Discrete channel model for a time-varying Wide Sense Stationary Uncorrelated Scattering (WSSUS) channel

The moduli of the complex tap gains, $a_k(t)$, are Rayleigh distributed

$$p[a_k] = \frac{a_k}{\sigma_k^2} e^{-\frac{{a_k}^2}{2\sigma_k^2}}, a_k \geq 0 \tag{2.4}$$

where $2\sigma_k^2$ is the power in the k^{th} path. The phases $\theta_k(t)$ have a uniform probability density functions given by

$$p[\theta_k] = \frac{1}{2\pi} \quad 0 \leq \theta_k \leq 2\pi \tag{2.5}$$

respectively. Later, we will consider Rician statistics for the first path. The PDF of the gain in case of Rician fading is given by

$$p[a_k] = \frac{a_k}{\sigma_k^2} e^{-\frac{{a_k}^2+C^2}{2\sigma_k^2}} I_0\left(\frac{C a_k}{\sigma_k^2}\right) \tag{2.6}$$

where C represents the power in the so-called specular component of the signal. Also, in the Rician case the joint PDF of the gain and phase is given by

$$p[a_k, \theta_k] = \frac{a_k}{2\pi\sigma_k^2} e^{-\frac{{a_k}^2+C^2-2rC\cos(\theta_k)}{2\sigma_k^2}} \tag{2.7}$$

2.2 The Coherent DLL

In figure 2-3 the traditional coherent DLL is shown. The DLL is a correlative tracking loop in which, the received signal is applied to two multipliers, where it is multiplied by two outputs from the local PN code generator. One of the outputs is delayed, while the other is advanced in time, with respect to incoming spreading waveform. Both of the early and late PN codes are delayed relative to each together by an amount less than or equal to a chip duration. Thus the product signals are the cross correlations between the received signals and the PN sequence at the two

values of delay. These products are band-pass filtered and then subtracted. This difference signal is low-pass filtered and fed to a Voltage Controlled Oscillator (VCO) which serves as the clock for the PN generator. If the synchronization is not exact, the filtered output from one correlator will exceed the other, and the VCO will be appropriately advanced or delayed. At the equilibrium point, the two filtered correlator output will be exactly synchronized to the received signal that is fed to the demodulator.

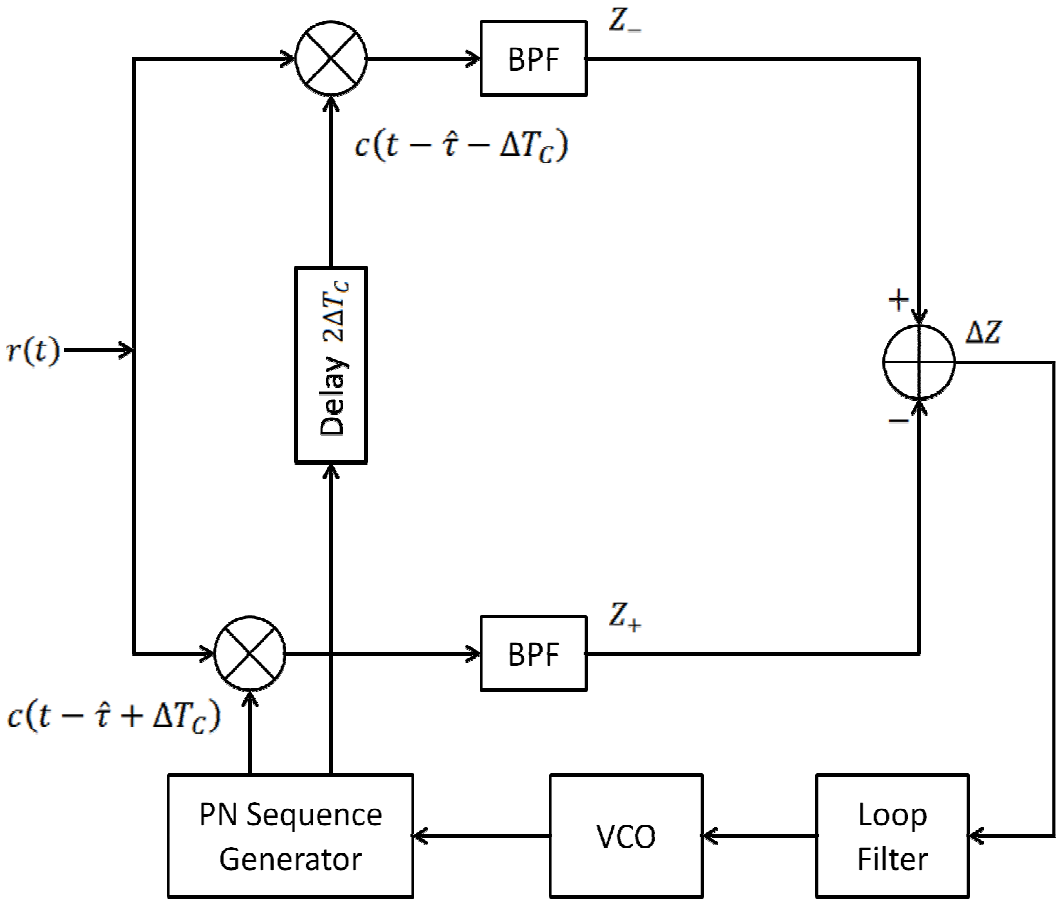

Figure 2-3: Traditional coherent DLL

2.3 RAKE-like Combining DLL

We present a performance analysis of the RAKE-like combining DLL introduced in [44]. The analysis given in [44] is extended in two respects: (1) We consider quadrature phase spreading and (2) We consider Rician fading in addition to Rayleigh fading channel models. The concept behind the RAKE-like combining DLL is of Maximum-Ratio Combining (MRC) that exploits the inherent multipath diversity of the channel. Diversity techniques are important methods to improve the transmission reliability of digital communication systems by combatting the effect of fading. Because of multiple signal propagation paths, copies of transmitted signals are sent over the fading channel from a transmitter. A receiver then combines these multiple copies to maximize the power of received signals. In maximum-ratio combining, each signal branch is multiplied by a weight factor that is proportional to the signal amplitude. That is, branches with strong signals are further amplified, while weak signals are attenuated. The weighted signals are then added together so that the output SNR can be maximized. The RAKE receiver consists of multiple correlators, in which the receive signal is multiplied by time-shifted versions of a locally generated code sequence. The intention is to separate signals such that each finger only sees signals coming in over a single (resolvable) path. After correlation, the signals are combined by using MRC. MRC is optimal for uncorrelated signal paths whose amplitudes are corrupted by AWGN [2]. Although RAKE combining is used for data detection, the same principle can be applied advantageously to signal parameter estimation as our results show.

The structure of the tracking loop is shown in Figure 2-4. The upper part of the Figure 2-4 is a channel-parameter estimation unit which consists of L+1 branches of gain-phase estimators. After despreading the received signal, the tap gains $a_k(t)$ and phases $\theta_k(t)$ are estimated by individual gain-phase estimators. The lower part of the figure is a coherent tracking loop that exploits the inherent multipath diversity of the channel. In each branch, say branch k, the received signal is first

correlated with the correlation function. The *correlation function* for the in-phase channel, $c_{I\Delta}(t - \hat{\tau} - kT_c)$, is made up of the difference of the early and late replicas of the delayed spreading function, i.e.

$$c_{I\Delta}(t - \hat{\tau} - kT_c) = c_I(t - \hat{\tau} - kT_c - \Delta T_c) - c_I(t - \hat{\tau} - kT_c + \Delta T_c) \tag{2.8}$$

where $0 < \Delta < 1$ is called the early-late discriminator offset. The correlation function of the quadrature phase channel is defined similarly:

$$c_{Q\Delta}(t - \hat{\tau} - kT_c) = c_Q(t - \hat{\tau} - kT_c - \Delta T_c) - c_Q(t - \hat{\tau} - kT_c + \Delta T_c) \tag{2.9}$$

The correlated signal is converted to baseband through multiplication with the recovered carrier which is given by $\hat{a}_k(t)\cos\left(\omega_c t + \hat{\theta}_k(t)\right)$ on the I channel and by $\hat{a}_k(t)\sin\left(\omega_c t + \hat{\theta}_k(t)\right)$ on the Q channel. The desired code phase error-correcting signal $e(t)$ is obtained by summing the low-pass filtered signals $y_{Ik}(t)$ and $y_{Qk}(t)$ from the individual branches. Finally, the loop is closed by low-pass filtering the error signal which is used to drive the voltage control clock (VCC) for correcting the code phase error of the local PN code.

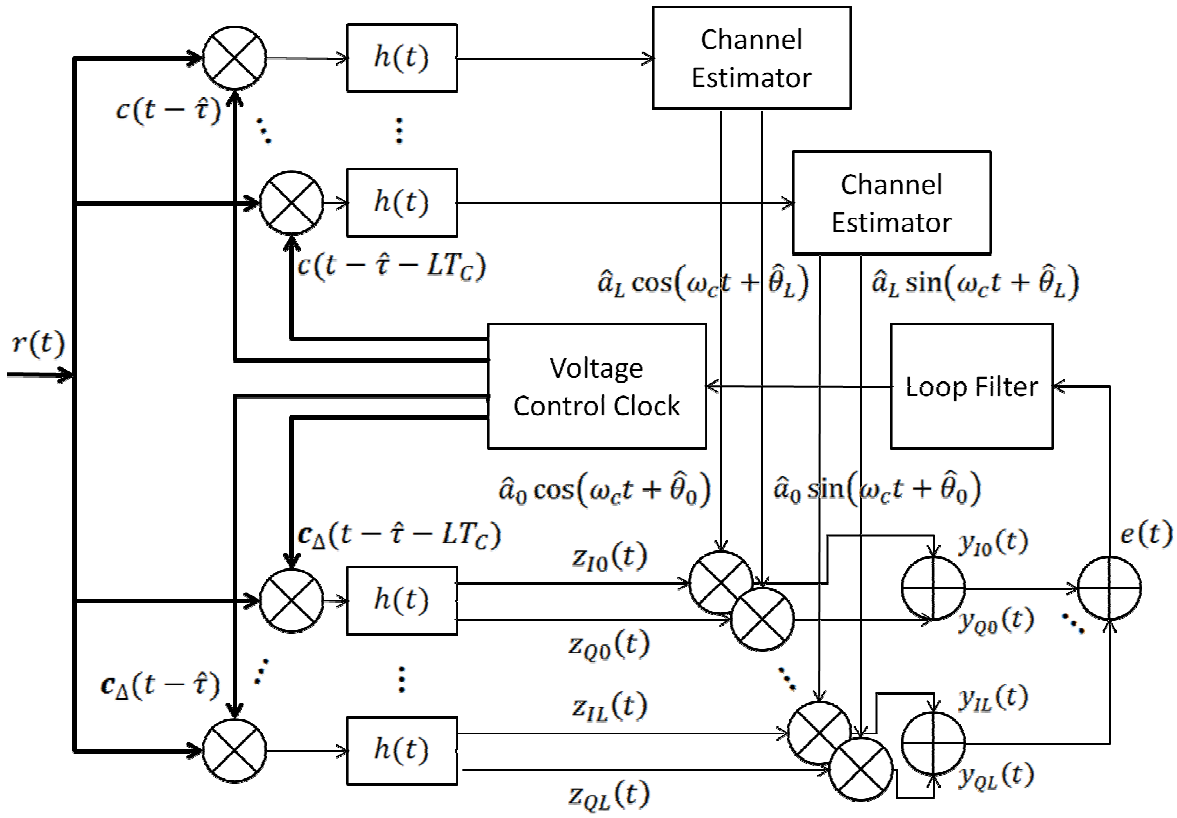

Figure 2-4: The RAKE-like combining DLL

A key feature of this tracking loop is the use of a RAKE-like correlator to resolve and combine (with maximal ratio combining) the received multipath components. As a result of the inherent multipath diversity, the tracking loop offers much better performance than the traditional DLL. The unresolved multipath components represent a strong source of interference for a traditional DLL, and they will cause significant performance degradation as shown in [44].

2.3.2 Stochastic Differential Equation (SDE) for the Combining DLL

The Stochastic Differential Equation (SDE) gives the loop tracking error behavior versus time. To solve for the tracking error statistics, it is necessary to first formulate the SDE for the combining

DLL. The associated Fokker-Plank equation can then be used to obtain the tracking error probability distribution.

The received signal after propagating through the multipath fading channel is given by:

$$r(t) = \sqrt{2P}\sum_{k} a_k(t)c_I(t-\tau(t)-kT_c)\cos\big(\omega_c t+\theta_k(t)\big) - a_k(t)c_Q(t-\tau(t)-kT_c)\sin\big(\omega_c t+\theta_k(t)\big)+n(t) \tag{2.10}$$

Here $a_k(t)$ are the channel fading coefficients, $\theta_k(t)$ is the received phase for the *k*th path, $c_I(t)$ is the spreading code for the in-phase channel and $c_Q(t)$ is the spreading code for the quadrature phase channel. The AWGN noise $n(t)$ is narrow-band noise process given by

$$n(t) = n_c(t)\cos(\omega_c t) - n_s(t)\sin(\omega_c t) \tag{2.11}$$

where $n_c(t)$ and $n_s(t)$ are independent, identically distributed, zero-mean Gaussian random variables with the same PSD as $n(t)$.

In the following analysis, we assume the following definition for the code autocorrelation:

$$R_C(\xi) = \frac{1}{NT_C}\int_0^{NT_C} c(t)c(t+\xi T_C)dt \tag{2.12}$$

The I and Q channels are multiplied with early-late difference of the respective PN sequences and then band-pass filtered. The resulting expression for the I Channel is at the output of the k^{th} band-pass filter is given as

$$z_{Ik}(t) = r(t)c_{I\Delta}(t - \hat{\tau} - kT_c) * h(t)$$
$$= \sum_m a_m \left(R_I(\varepsilon + m - k - \Delta) - R_I(\varepsilon + m - k + \Delta)\right) \cos(\omega_c t + \theta_m) + n_I(t) \quad (2.13)$$

The cross terms involving I and Q channel PN codes vanish because of bandpass filtering. In equation 2.19 the normalized error ε is defined as:

$$\varepsilon = \frac{\tau(t) - \hat{\tau}(t)}{T_C} \quad (2.14)$$

Also, the total noise on the I channel after correlation becomes

$$n_I(t) = n_{Ik}^c(t)\cos(\omega_c t) - n_{Ik}^s(t)\sin(\omega_c t) \quad (2.15)$$

where

$$n_{Ik}^c(t) = n_c(t)c_{I\Delta}(t - \hat{\tau} - kT_c) * \tilde{h}(t) \quad (2.16)$$

$$n_{Ik}^s(t) = n_s(t)c_{I\Delta}(t - \hat{\tau} - kT_c) * \tilde{h}(t) \quad (2.17)$$

with $\tilde{h}(t)$ denoting the equivalent lowpass impulse response of the BPF, and $*$ denoting the convolution operator. In 2.13 the PN code self-noise has been neglected, because the bandwidth of the BPF is assumed to be much smaller than the chip rate $1/T_C$ [9]. In 2.14, ε is a function of t. However, for notational simplicity t will be omitted in the sequel. A similar expression occurs for the Q channel after code correlation and band pass filtering:

$$z_{Qk}(t) = r(t)c_{Q\Delta}(t - \hat{\tau} - kT_c) * h(t)$$
$$= \sum_m a_m \left(R_Q(\varepsilon + m - k - \Delta) - R_Q(\varepsilon + m - k + \Delta)\right) \sin(\omega_c t + \theta_m) + n_Q(t) \quad (2.18)$$

Both $R_Q(\cdot)$ and $R_I(\cdot)$ are the same for maximal length sequences having the same period. For a large code period N and a root raised cosine chip shaping function, the code autocorrelation function is given by [46]:

$$R_{Q,I}(\xi) = \frac{\sin\left(\frac{\pi\xi}{T_C}\right)}{\frac{\pi\xi}{T_C}} \frac{\cos\left(\frac{0.22\pi\,\xi}{T_C}\right)}{1-\left(\frac{.44\xi}{T_C}\right)^2} \tag{2.19}$$

Both I and Q channels are then down converted at each of channel taps. The resulting signal for the I channel is given by

$$\begin{aligned} y_{Ik}(t) = \sqrt{\frac{P}{2}} \sum_m \hat{a}_k a_m \big(R_I(\varepsilon + m - k - \Delta) \\ - R_I(\varepsilon + m - k + \Delta)\big) \cos(\omega_c t + \theta_m) \cos\big(\omega_c t + \hat{\theta}_k\big) + \hat{a}_k n_I(t) \cos\big(\omega_c t + \hat{\theta}_k\big) \\ = \sqrt{\frac{P}{2}} \sum_m a_k a_m \big(R_I(\varepsilon + m - k - \Delta) - \ R_I(\varepsilon + m - k + \Delta)\big) \cos(\theta_m - \theta_k) \\ + \frac{1}{\sqrt{2}} a_k \underbrace{n_I(t) \cos(\omega_c t + \theta_k)}_{w_{Ik}(t)} \end{aligned}$$

Because perfect channel estimates are available, $\hat{a}_k = a_k$. The noise term $w_{Ik}(t)$ is given as:

$$\begin{aligned} w_{Ik}(t) &= n_I(t) \cos(\omega_c t + \theta_k) \\ &= n_{Ik}^c(t) \cos(\theta_k) + n_{Ik}^s \sin(\theta_k) \end{aligned} \tag{2.20}$$

A similar expression can be derived for the Q channel. It is given by

$$y_{Qk}(t) = \sqrt{\frac{P}{2}} \sum_{m} a_k a_m \Big(R_Q(\varepsilon + m - k - \Delta) - \ R_Q(\varepsilon + m - k + \Delta) \Big) \cos(\theta_m - \theta_k)$$

$$+ \frac{1}{\sqrt{2}} a_k \underbrace{n_Q(t) \sin(\omega_c t + \theta_k)}_{w_{Qk}(t)}$$

Finally the error signal is fed to the VCC that derives the PN code generators for both I and Q channels. The error signal is given by

$$\begin{aligned} e(t) &= \sum_{k=0}^{L} \Big(y_{Ik}(t) + y_{Qk}(t) \Big) \\ &= \sqrt{\frac{P}{2}} S(\varepsilon) + n_T(t) \end{aligned} \tag{2.21}$$

where $S(\varepsilon)$ is the S-curve for the code tracking loop and $n_T(t)$ is the total noise. The S-curve can be computed by substituting the expressions for $y_{Ik}(t)$ and $y_{Qk}(t)$ in Equation 2.21,

$$S(\varepsilon) = 2 \sum_{k=0}^{L} \sum_{m=0}^{L} a_k a_m \big(R_I(\varepsilon + m - k - \Delta) - R_I(\varepsilon + m - k + \Delta) \big) \cos(\theta_m - \theta_k) \tag{2.22}$$

The total noise is give by

$$n_T(t) = \frac{1}{\sqrt{2}} \sum_{k=0}^{L} a_k \left(w_{Ik}(t) + w_{Qk}(t) \right) \tag{2.23}$$

where:

$$\begin{aligned} w_{Qk}(t) &= n_Q(t)\sin(\omega_c t + \theta_k) \\ &= n_{Qk}^{c}(t)\sin(\theta_k) - n_{Qk}^{s}\cos(\theta_k) \end{aligned} \tag{2.24}$$

The expression for $w_{Ik}(t)$ is given in 2.20. A factor of two occurs in 2.22 because the autocorrelation for the PN sequences on both the I and Q channel is the same.

As shown in Figure 2-4, the error signal at the output of the loop filter is used to drive a VCO for correcting the code phase error. The operation of the VCO is described by the equation

$$\frac{\hat{\tau}(t)}{T_C} = k_L \int_0^t f(t') * e(t')dt' \tag{2.25}$$

where k_L is gain of the VCO, and $f(t)$ is the impulse response of the loop filter. Combining 2.21 and 2.25 gives the following stochastic differential equation (SDE) which describes the dynamic behavior of the tracking loop:

$$\frac{d\varepsilon}{dt} = -k_L \left\{ \sqrt{\frac{P}{2}} S(\varepsilon) + n_T(t) \right\} * f(t) \tag{2.26}$$

Because the channel is slowly time varying, the code Doppler shift is zero. For simplicity only the first order code tracking loop will be considered. Thus the SDE in 2.26 becomes

$$\begin{aligned} \frac{d\varepsilon}{dt} &= -k_L \left\{ \sqrt{\frac{P}{2}} S(\varepsilon) + n_T(t) \right\} * \delta(t) \\ &= -k_L \left\{ \sqrt{\frac{P}{2}} S(\varepsilon) + n_T(t) \right\} \end{aligned} \tag{2.27}$$

2.4 Nonlinear analysis using the Fokker-Plank Method

We intend to solve for the PDF of the tracking error process ε. The solution to a problem of this nature is usually obtained by assuming that the noise process driving the system is wideband compared to the system bandwidth, in which case the error process can be assumed to be Markovian and its probability density function is a solution to a Fokker-Plank equation associated with its stochastic differential equation (SDE) [45]. The Fokker-Plank equation is a differential equation that first arose in connection with the statistics of Brownian motion of particles suspended in water. It has found application in synchronization systems for communication such as phase-lock loops and correlative tracking loops. Here we present the Fokker-Plank equation without giving further details on its derivation. For a general review of the Fokker-Plank equation together with its solution, the reader is referred to Appendix A.

Before we proceed, the following definitions are useful.

(i) $\mathcal{R} \triangleq (\varepsilon_{min}, \varepsilon_{max})$: the in-lock region of the loop, i.e., if $\varepsilon \in \mathcal{R}$, then the code acquisition unit declares an in-lock condition and switches the synchronization process to the tracking unit.

(ii) $P_{LD}(\varepsilon)$: The probability that the tracking unit declares an out-of-lock condition when the tracking error is still within the in-lock region $\mathcal{R}$. The boundaries are absorbing, i.e., $P_{LD}(\varepsilon_{max}) = P_{LD}(\varepsilon_{min}) = 1$.

(iii) $\pi(\varepsilon)$: The initial PDF of the code timing error when the synchronization process is switched from the acquisition unit to the tracking unit.

Let $p(\varepsilon|\boldsymbol{g})$ be the stationary PDF of the tracking error for a given channel $\boldsymbol{g} = [a_1, a_2, \theta_1, \theta_2]$. Then, by the assumption that the correlation time of $n_T(t)$ is much smaller than the inverse of the loop bandwidth, (or equivalently that the system bandwidth is smaller than the bandwidth of the

noise process $n_T(t)$) the following Fokker-Plank is satisfied by $p(\varepsilon|\boldsymbol{g})$ with boundary conditions $p(\varepsilon_{min}|\boldsymbol{g}) = p(\varepsilon_{max}|\boldsymbol{g}) = 0$ [34],

$$\frac{\partial}{\partial\varepsilon}\left[\frac{k_1(\varepsilon)p(\varepsilon|\boldsymbol{g})}{P_D(\varepsilon)}\right] - \frac{1}{2}\frac{\partial^2}{\partial\varepsilon^2}\left[\frac{k_2 p(\varepsilon|\boldsymbol{g})}{P_D(\varepsilon)}\right] = \frac{\pi(\varepsilon)}{\mathrm{E}[\tau^{tr}|\boldsymbol{g}]} \tag{2.28}$$

where $P_D(\varepsilon) = 1 - P_{LD}(\varepsilon)$, $\mathrm{E}[\tau^{tr}|\boldsymbol{g}]$ is the conditional mean time for the tracking error process to hit either of the boundaries ε_{min} or ε_{max} (i.e., for the loop to enter an out of lock condition). The intensity coefficients $k_1(\varepsilon)$ and k_2 are given by

$$k_1(\varepsilon) = -k_L\sqrt{\frac{P}{2}}S(\varepsilon) \tag{2.29}$$

$$\begin{aligned} k_2 &= k_L^2\int_{-\infty}^{\infty} R_{n_T}(\xi)d\xi \\ &= k_L^2\int_{-\infty}^{\infty} E[n_T(t)n_T(t+\xi)]d\xi \end{aligned} \tag{2.30}$$

The above expressions for the intensity coefficients $k_1(\varepsilon)$ and k_2 are obtained from the stochastic differential equation 2.27 by inspection using the rules of Ito Calculus [45]. To solve the associated Fokker-Plank equation for $p(\varepsilon|\boldsymbol{g})$ we need to evaluate the integral of the autocorrelation function of the total noise $n_T(t)$ which is k_2. Using some algebraic manipulation, the expression for k_2 is derived in Appendix B. In the Fokker-Plank equation 2.28, the conditional PDF $p(\varepsilon|\boldsymbol{g})$ can be computed using the standard techniques (separation of variables) of solving differential equations (see [51]) to give,

$$p(\varepsilon|\boldsymbol{g}) = \frac{Q(\varepsilon|\boldsymbol{g})}{E[\tau^{tr}|\boldsymbol{g}]}, \qquad \varepsilon_{min} \le \varepsilon \le \varepsilon_{max} \tag{2.31}$$

where

$$Q(\varepsilon|\boldsymbol{g}) = 2P_D(\varepsilon)\frac{\exp\left[-u_0(\varepsilon)\right]}{k_2}\int_{\varepsilon_{min}}^{\varepsilon}\left[d_0 - \Pi(x)\right]\exp\left[u_0(x)\right]dx \tag{2.32}$$

with

$$u_0(\varepsilon) = -2\int_{\varepsilon_{min}}^{\varepsilon}\frac{k_1(x)}{k_2}\,dx \tag{2.33}$$

$$d_0(\varepsilon) = \frac{\int_{\varepsilon_{min}}^{\varepsilon_{max}}\Pi(x)\exp\left[u_0(x)\right]dx}{\int_{\varepsilon_{min}}^{\varepsilon_{max}}\exp\left[u_0(x)\right]dx} \tag{2.34}$$

$$\Pi(\varepsilon) = \int_{\varepsilon_{min}}^{\varepsilon}\pi(x)\,dx \tag{2.35}$$

$$E[\tau^{tr}|\boldsymbol{g}] = \int_{\varepsilon_{min}}^{\varepsilon_{max}}Q(\varepsilon|\boldsymbol{g})\,dx \tag{2.36}$$

For this analysis, the initial code phase $\pi(\varepsilon)$ is taken as $\delta(\varepsilon)$, where $\delta(\cdot)$ is the Dirac Delta function. This implies that

$$\Pi(\varepsilon) = u(\varepsilon) \tag{2.37}$$

where $u(\varepsilon)$ is the unit step function. Also, $d_0(\varepsilon)$ is evaluated as

$$d_0(\varepsilon) = \frac{1}{2} \tag{2.38}$$

Here we have used the fact that $u_0(-x) = u_0(x)$ or that the *potential function* $u_0(x)$ is even.

Using 2.31, the PDF of the steady state normalized tracking error can be calculated as:

$$p(\varepsilon) = \int p(\varepsilon|\boldsymbol{g})p(\boldsymbol{g})\, d\boldsymbol{g} = \int \frac{Q(\varepsilon|\boldsymbol{g})}{E[\tau^{tr}|\boldsymbol{g}]} p(\boldsymbol{g}) d\boldsymbol{g} \tag{2.39}$$

where $p(\boldsymbol{g})$ is the PDF of the channel impulse response. In our analysis, we consider a two-tap channel with gains a_1, a_2 and phases θ_1, θ_2. Thus the limits on the integral in 2.39 become

$$p(\varepsilon) = \int_0^{2\pi}\int_0^{2\pi}\int_0^{\infty}\int_0^{\infty} \frac{Q(\varepsilon|a_1, a_2, \theta_1, \theta_2)}{E[\tau^{tr}|a_1, a_2, \theta_1, \theta_2]} p(a_1)p(a_2)p(\theta_1)p(\theta_1)\, da_1 da_2 d\theta_1 d\theta_2 \tag{2.40}$$

2.5 Numerical Results

The integral in 2.40 is a complicated integral in multiple dimensions (in our case, a four dimensional integral for a two tap channel) and it is evaluated by using Monte Carlo integration with 10^5 samples. A two-path channel is considered, so that the numerical computations remain tractable. The tracking loops are evaluated in terms of the averaged received SNR γ_b, the averaged nominal loop bandwidth B_{L0} and the power ratio R of the first and second channel taps. These parameters are defined as follows:

$$R = \frac{E[a_0^2]}{E[a_1^2]} \tag{2.41}$$

$$\gamma_b = PT_b\left\{\frac{E[a_0^2] + E[a_1^2]}{N_0}\right\} \tag{2.42}$$

$$\begin{aligned} B_{L0} &= \frac{k_L}{4}\sqrt{\frac{P}{2}}\mathrm{E}\{S'(\varepsilon)|_{\Delta=1/2}\} \\ &= \frac{k_L}{2}\sqrt{\frac{P}{2}}E[a_0^2]\left\{1 + \frac{1}{R}\right\} \end{aligned} \tag{2.43}$$

where P is the average received power, T_b is the bit duration k_L is the gain of the VCO and $S'(\varepsilon)$ is the derivative of the S-curve for the DLL given by Equation 2.22.

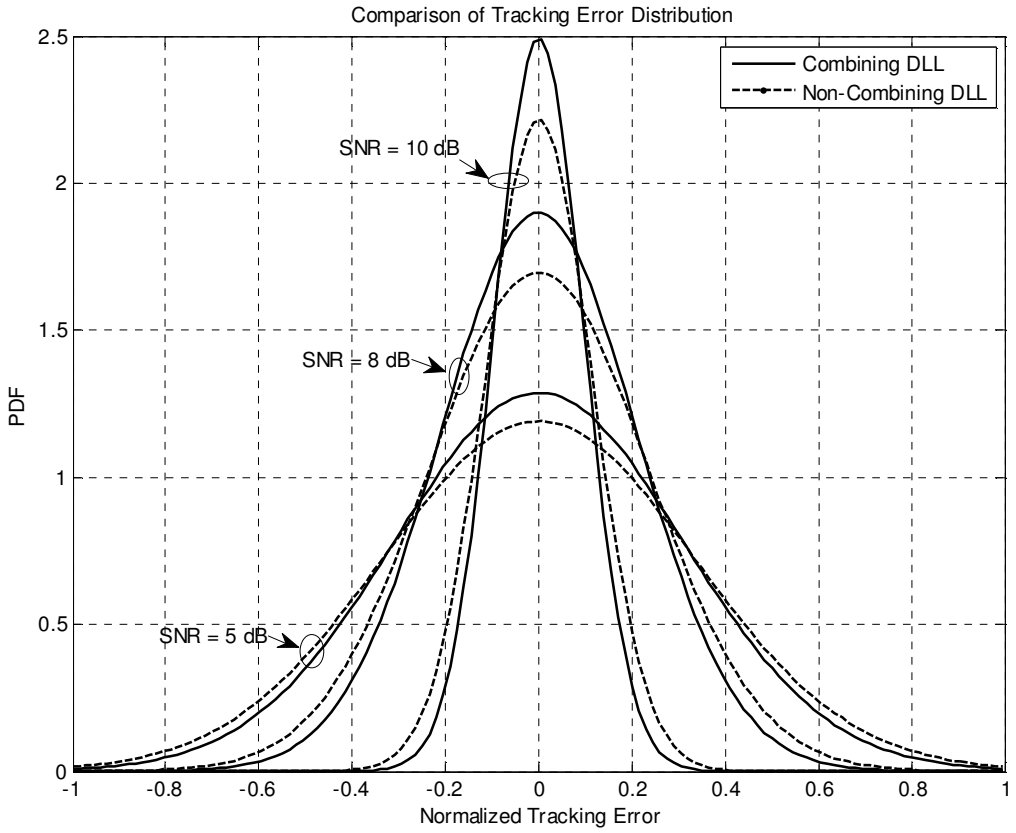

Figure 2-5: Comparison of Tracking Error PDFs for Combining and Non-Combining DLL under Rayleigh Fading with early-late offset of 0.5, R=2

Figure 2-5 compares the PDFs of the normalized tracking error for RAKE-like combining and non-combining DLLs under Rayleigh fading conditions for SNRs of 5 dB, 8 dB and 10 dB. The ratio of power in the first path to the power in the second path is 3 dB. We see that the PDFs for the combining DLL have a lower variance than those for the non-combining DLL at all SNRs. The lower variance PDFs for the combining DLL indicate that resulting ToA measurements are more accurate. Note that the effect (sharpened PDFs) is more pronounced (the difference between PDF peaks is larger) at higher SNR than at low SNRs. This trend is corroborated further by the results in

Figure 2-8 and Figure 2-9 where the mean square tracking error is plotted against the SNR for both DLLs.

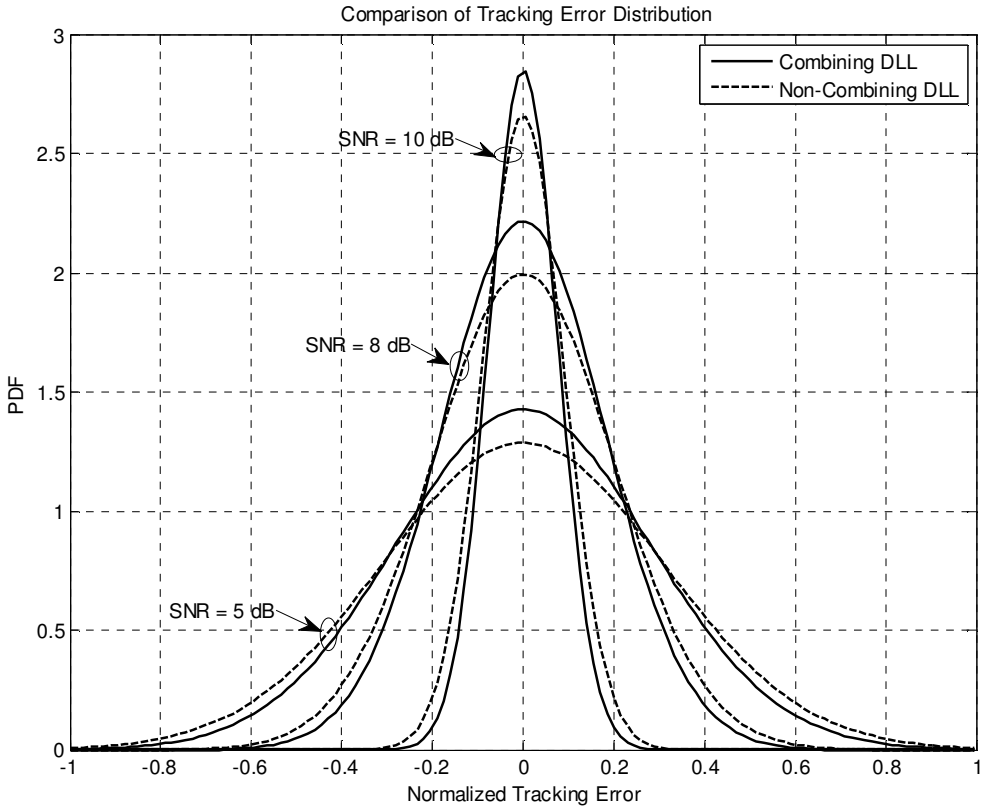

Figure 2-6: Comparison of Tracking Error PDFs for Combining and Non-Combining DLL under Rician Fading with early-late offset of 0.5 and a Rice factor of 5

Figure 2-6 compares the PDFs of the normalized tracking error for RAKE-like combining and non-combining DLLs under Rician fading conditions for SNRs of 5 dB, 8 dB and 10 dB. The ratio of power in the first path to the power in the second path is 3 dB. An early-late offset of 0.5 is used. Again, as in Figure 2-5 we see that the PDFs for the combining DLL have a lower variance than those for the non-combining DLL at all SNRs. We note that for the Rician case the difference

between the peaks of the PDFs for the combining and non-combining PDFs does not increase for at least this range of SNRs. The PDF calculations were done for a Rice factor of 5.

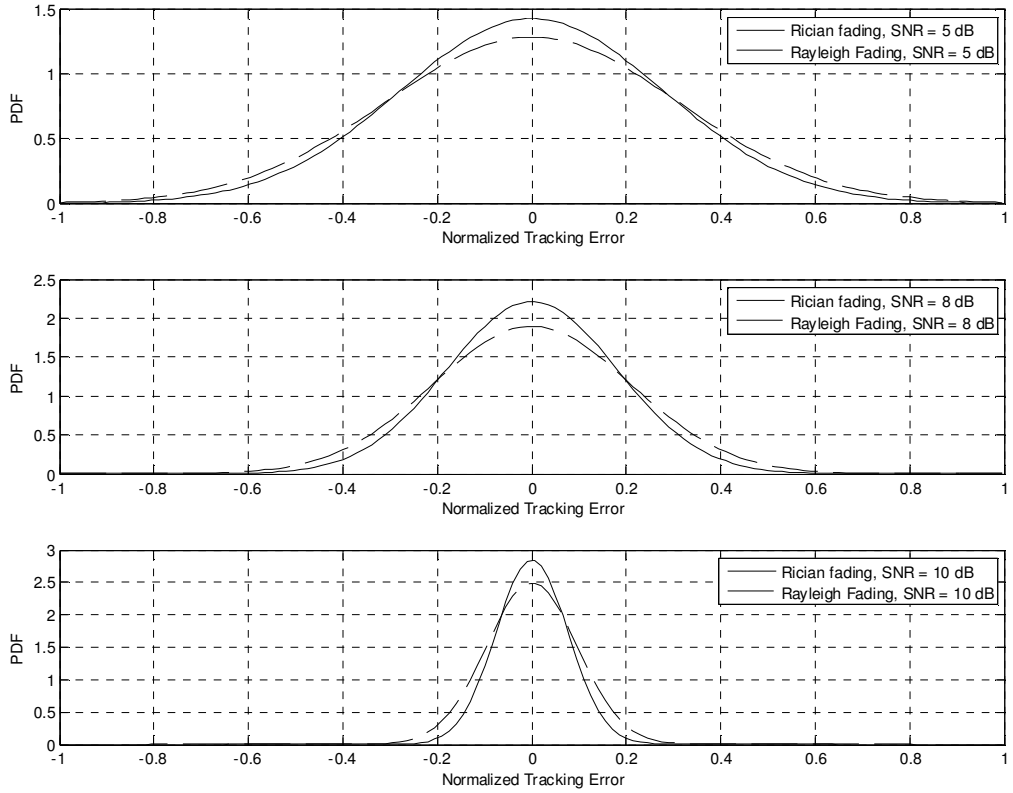

Figure 2-7: Comparison of tracking error PDFs for the combining DLL under Rayleigh and Rician fading, with early-late offset of 0.5 and using a Rice factor of 5.

Figure 2-7 gives a comparison of the PDFs of normalized tracking error for the RAKE-like combining DLL under Rayleigh and Rician fading. The PDFs are computed for SNRs of 5 dB, 8 dB and 10 dB. We see that, because of the "specular" signal component present in the case of Rician fading, the PDFs have a lower variance than that for Rayleigh fading. Also as the SNR

increases the difference between the peaks of the PDF for the two cases increases. The early late offset us 0.5 and the Rice factor used for the calculation of the PDFs is 5.

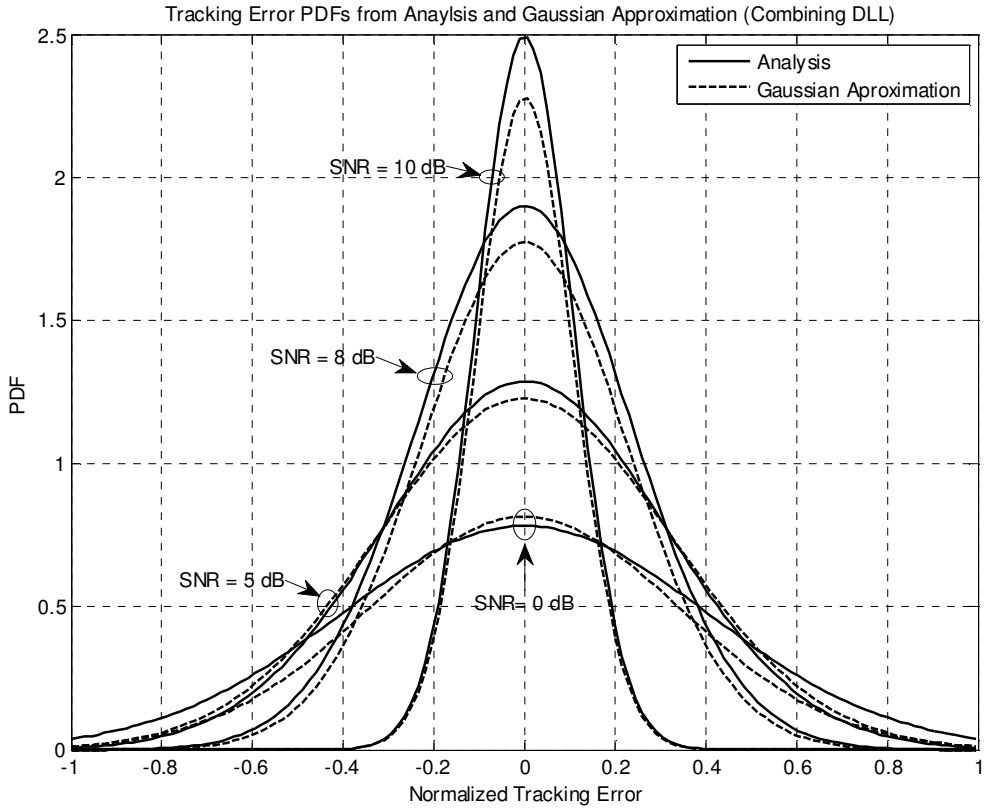

Figure 2-8: Comparison of tracking error PDFs from analysis and Gaussian approximation for the RAKE-like combining DLL (Rayleigh Fading, early-late offset of 0.5)

Figure 2-8 compares the PDFs of the normalized tracking error for RAKE-like combining and the corresponding Gaussian approximations under Rayleigh fading conditions for SNRs of 0 dB, 5 dB, 8 dB and 10 dB. The ratio of power in the first path to the power in the second path is 3 dB. It is seen that the Gaussian Approximation gives pessimistic results for high SNRS (> 0 dB). The curvature of the Gaussian approximated PDF is lower than that for the true PDF. At low SNRs (0 dB) the Gaussian approximation gives optimistic results as the curvature of the Gaussian PDF is higher than that for the true PDF.

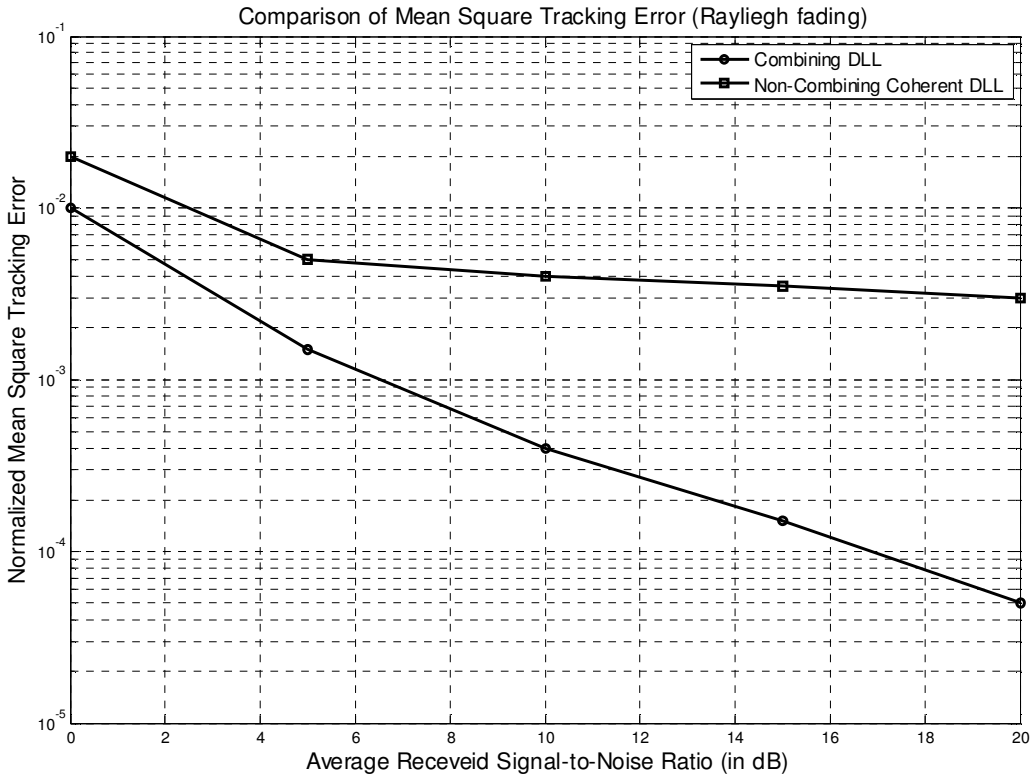

Figure 2-9: Comparison of Mean Square Tracking Error for the combining DLL and traditional DLLs under Rayleigh fading

Figure 2-9 compares the variance of the normalized tracking error for the combining DLL and the non-combining DLL, under Rayleigh fading conditions. The power ratio of the first path to the second is 3 dB. We see that in terms of the mean square tracking error the combining DLL outperforms the conventional, non-combining DLL at all values of SNR. Note that at low SNRs (2-4 dB) the performance difference between the two DLLs is small (the mean square tracking error for the combining DLL is half of that for the non-combining one), but at high SNRs a performance floor emerges for the non-combining DLL while the combining DLL continues to show improvement in mean square tracking with the increase in SNR. So, for example, the difference in performance at 20 dB is of several orders of magnitude.

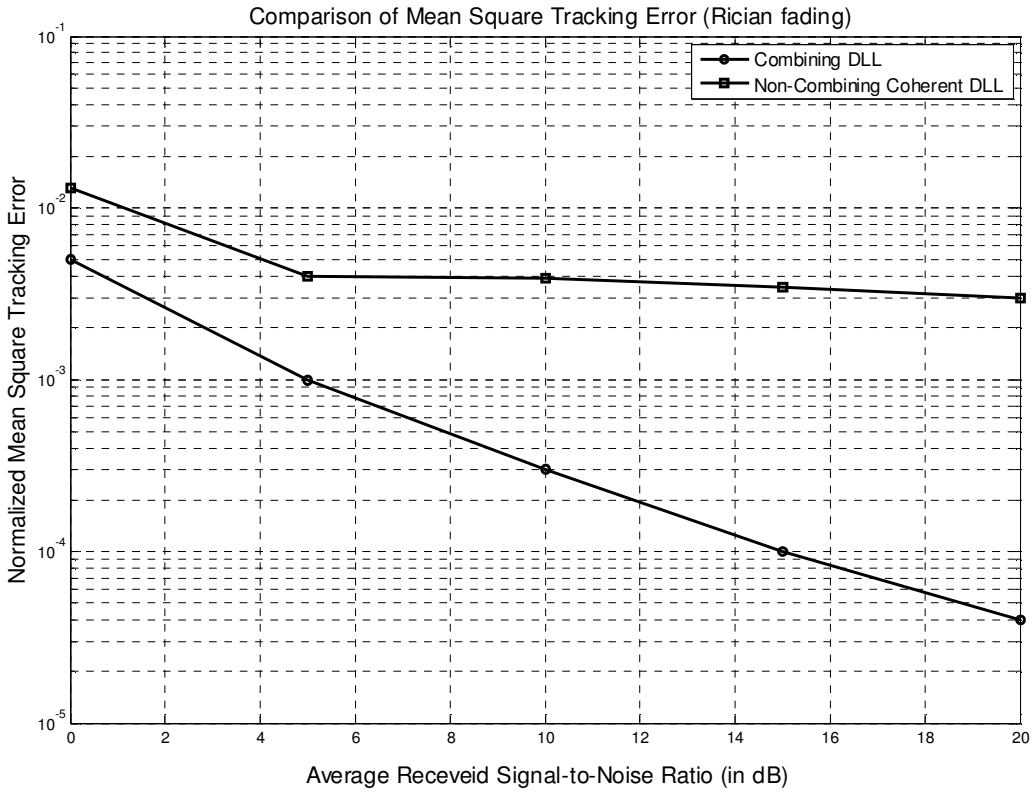

Figure 2-10: Comparison of Mean Square Tracking Error for the combining DLL and traditional DLLs under Rician fading (K factor of 5)

Figure 2-10 compares the variance of the normalized tracking error for the combining DLL and the non-combining DLL, under Rician fading conditions. The Rice factor used for the calculation of the mean square tracking error is 5. Again, we see that the combining DLL overwhelmingly outperforms the non-combining DLL at all values of SNR. The difference in performance between the DLLs increases significantly as SNR is increased. At 20 dB the difference in performance is about a hundred times. Also there is a persistent performance floor that emerges for the non-combining DLL at high SNRs, while the combining DLL continues to show a performance increase as the SNR is increased.

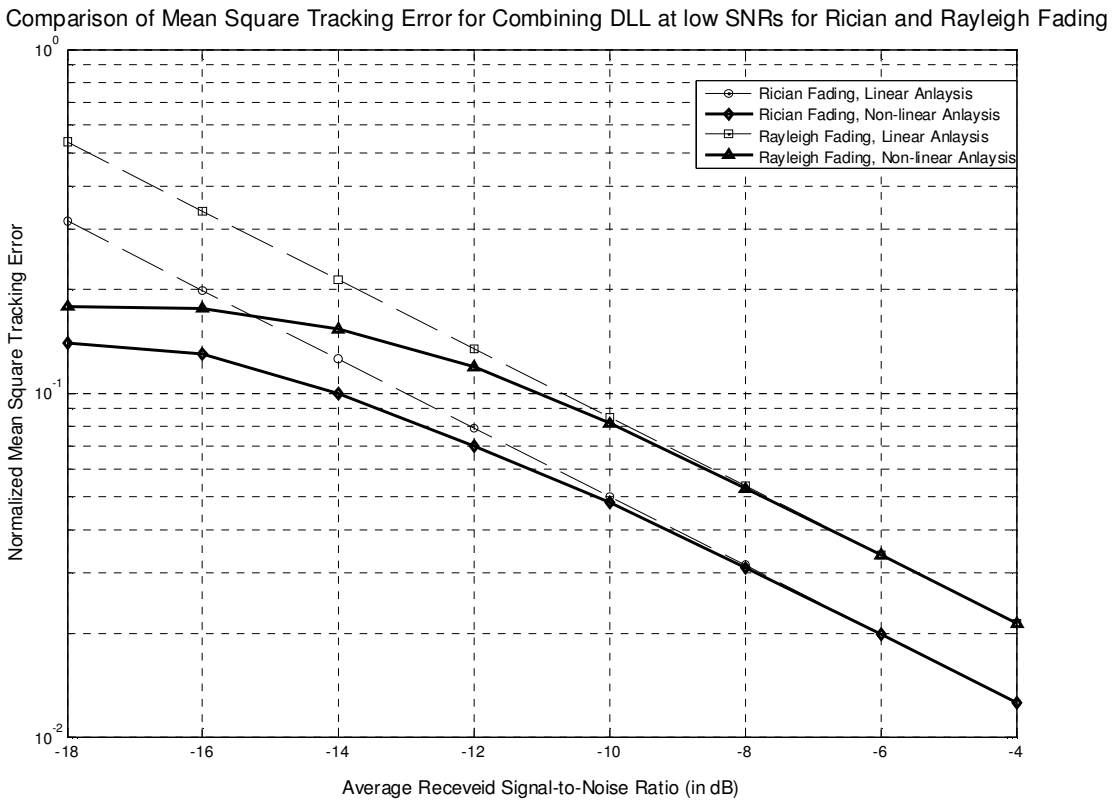

Figure 2-11: Comparison of MSE Error for the Combining DLL Rician fading and Rayleigh for low SNRs. Dashed curves show approximate linearized analysis obtained in [44].

Figure 2-11 compares the variance of the normalized tracking error of the combining DLL under Rayleigh and Rician fading in the low SNR regime (-18 dB to -4 dB). The solid curves are obtained by using the Fokker-Plank analysis of this chapter. The dashed curves give the linear analysis found in [44]. From the linear analysis, the formula for the normalized tracking error variance (for Rayleigh fading) is given by

$$\sigma_\varepsilon^2 = \frac{B_{L0} T_b}{2\gamma_b} \tag{2.44}$$

where T_b is the bit duration and B_{L0} (nominal loop bandwidth) and γ_b (averaged received SNR) are defined in equations 2-42 and 2-43 respectively. For Rician fading the mean square tracking error (from linear analysis) is given by:

$$\sigma_\varepsilon^2 = \frac{B_{L0} T_b}{0.68\, K\, \gamma_b} \tag{2.45}$$

where K is the Rice factor. We note that for SNR values greater than -12 dB the linear and non-linear analysis agree closely, however for SNR values below this threshold the linear theory gives overly pessimistic results.

2.6 Summary and Conclusion

A detailed performance analysis of the RAKE-like combining DLL was carried out. Full first order statistics of the tracking error process for the DLL were obtained. The performance analysis was done for quadrature phase modulation and spreading, taking into account multipath fading in a frequency selective channel. A two-path Rician/Rayleigh fading channel was considered. The tracking error statistics were obtained by using the Fokker-Plank method which caters for the non-linearity of the loop, avoiding any linearization of the loop equation that is usually done as an approximation (also, the approximation can be used to compute the variance of the tracking error only). The solution to the Fokker-Plank equation was obtained through Monte-Carlo integration of a high-dimensional integral. Our results show that, in the low SNR regime, linear analysis provides overly optimistic results for the mean squared tracking error of the combing DLL. For high SNRs, the non-linear and linear methods converge to give the same values for the mean squared tracking error. The tracking error PDF for a conventional, non-combining DLL under multipath fading were compared with those of the combining DLL. Significant improvement was seen in performance for

the combining DLL at all values of SNR. We note that for high SNRs an error floor emerges for the traditional DLL, whereas the combining DLL continues to show performance gains as SNR is increased.

Chapter 3 Code Tracking by Noncoherent DLL

In the last chapter we considered a RAKE-like multi-DLL structure that operated coherently. Since the modulation was coherent, a coherent carrier reference must be generated prior to demodulation, hence the need for channel gain and phase estimators for each path. This leads to increased implementation complexity. In addition, the generation of this coherent reference at extremely low signal-to noise ratios is difficult. Neither of these difficulties are present for the noncoherent delay-lock tracking loop that we explain next. The noncoherent loop employs a phase discriminator which is significantly different from that used in the coherent DLL. The discriminator contains two energy detectors, which are not sensitive to carrier phase and thus enable the discriminator to ignore carrier phase.

In this chapter, the performance of first-order noncoherent digital delay lock loops (DDLL) for direct-sequence spread spectrum (DS-SS) signals is investigated under multipath Rayleigh fading. We will consider quadrature spread signals, keeping in view the 3G UMTS standards. The steady-state probability distribution for the timing error of the first-order loop for DS-SS signals in Rician fading environment is computed, and the results are compared with a Rayleigh fading channel.

The chapter is organized as follows. We first present the channel model used for the performance analysis of the QPSK non-coherent digital DLL. We then consider the overall system model for the DLL. The model takes into account quadrature spreading and multipath fading. The expression for the discriminator output of the DLL is then obtained. The discriminator output is expressed as a function of the S-curve of the loop. Subsequently, the Stochastic Difference Equation (SDE) that describes the dynamics of the discrete time tracking error process is developed for the Rayleigh

fading channel. The SDE that describes the tracking error process shows that the process is first order Markovian. Such a process is completely described by its one-step transition probability density function. A closed-form expression for this transition pdf is obtained for a Rayleigh fading. channel. For Rician fading, a closed-form expression for the transition pdf cannot be obtained. Resort is made to numerical methods. Finally, the steady state pdf of the tracking error is iteratively computed by using the initial pdf, the transition pdf and the Kolmogorov-Chapman equation.

3.1 Multipath Channel Model

For this analysis a frequency-selective multipath channel is considered. For a discrete multipath channel, the complex lowpass impulse response can be expressed as

$$h(\tau;\, t) = \sum_{n=-\infty}^{\infty} g_n e^{j\theta_n} \delta(\tau - \tau_n) \tag{3.1}$$

where

$$g_n = \sqrt{(A_n + a_{nR})^2 + a_{nI}^2} \tag{3.2}$$

and

$$\theta_n = Tan^{-1}\left(\frac{a_{nI}}{A_n + a_{nR}}\right) \tag{3.3}$$

are respectively the attenuation and phase associated with the *n*th path. For the general case, A_n represents the specular component from the direct path, and a_{nR} and a_{nI} represent the real and imaginary diffuse components (the diffuse component appears as a complex number because we are considering a baseband representation). Throughout this analysis, the specular component is

present for the first path only (for $n = 0$) and $A_n = 0$ for the subsequent paths. $\tau_n(t)$ is the associated time delay for the *n*th path and is taken to be non-random.

The diffuse components are the net effect of a large number of independent paths at a given delay τ_n. Thus, by applying the Central Limit Theorem, they can be modeled as uncorrelated zero-mean Gaussian processes. Since a_{nR} and a_{nI} are zero-mean IID Gaussian random variables, g_n can be modeled as Rician distributed with PDF

$$p(g_n) = \frac{g_n}{\sigma_n^2} \exp\left(-\frac{g_n^2 + A_n^2}{2\sigma_n^2}\right) I_0\left(\frac{g_n A_n}{\sigma_n^2}\right), \quad g_n \geq 0 \tag{3.4}$$

Where $\sigma_n^2 = E[a_{nR}^2] = E[a_{nI}^2]$, $I_0(\cdot)$ is a zeroth order modified Bessel function of the first kind and $E[\cdot]$ denotes the expectation operation. In our case only the first path has a specular component and consequently all subsequent paths are Rayleigh-distributed with

$$p(g_n) = \frac{g_n}{\sigma_n^2} \exp\left(-\frac{g_n^2}{2\sigma_n^2}\right), \quad g_n \geq 0 \tag{3.5}$$

3.2 System Model for DLL ToA Tracking

We consider a DS/SS system employing the quaternary phase-shift keying (QPSK) modulation and complex spreading. The model is constructed to analyze DLL for signal time of arrival (ToA) at the receiver. The complex baseband signal can be expressed as

$$\tilde{s}(t) = \sqrt{\beta/2} \sum_{m=-\infty}^{\infty} d_{\lfloor m \rfloor_L} c_{m\ (mod\ N)}\, h(t - m\,T_c) \tag{3.6}$$

where $\lfloor m \rfloor_L \stackrel{\text{def}}{=} int\left[\frac{m}{L}\right]$ and L and N denote respectively the spreading factor and the period of the spreading code. β is the transmitted signal power, $\{d_m\}$ is the complex data symbol (because there is no data modulation, $d_m = 1$ for all m), $\{c_m\}$ is the complex scrambling code sequence, $h(t)$ is the impulse response of a pulse shaping filter, and T_c is the chip duration.

In frequency-selective fading environments, the received signal at the output of the radio frequency (RF) bandpass filter can be written as

$$r(t) = \sqrt{\beta/2}\Re\mathrm{e}\left[\sum_{i=1}^{M} \tilde{s}\big(t - \tau_i(t)\big)a_i(t)e^{j2\pi f_c t}\right] + n(t) \tag{3.7}$$

where M is the number of resolvable multipath signals, $a_i(t)$ and $\tau_i(t)$ are respectively the complex channel amplitude and propagation delay of the i^{th} path signal, and f_c is the carrier frequency. As before (in chapter 2) the channel amplitudes $a_i(t)$ are independent random processes. The noise $n(t)$ is given by

$$n(t) = n_c(t)\cos\big(2\pi f_c t\big) - n_s(t)\sin\big(2\pi f_c t\big) \tag{3.8}$$

where $n_c(t)$ and $n_s(t)$ are zero-mean independent Gaussian random processes, each having the same power $N_0 W$. The spectral density due to thermal noise and signal bandwidth are respectively denoted by N_0 and W. It is assumed that other path signals are separated from the path signal under tracking by more than $1.5T_c$. In this case, other path signals can be regarded as the interference that simply increases the interference-plus-noise spectral density [46].

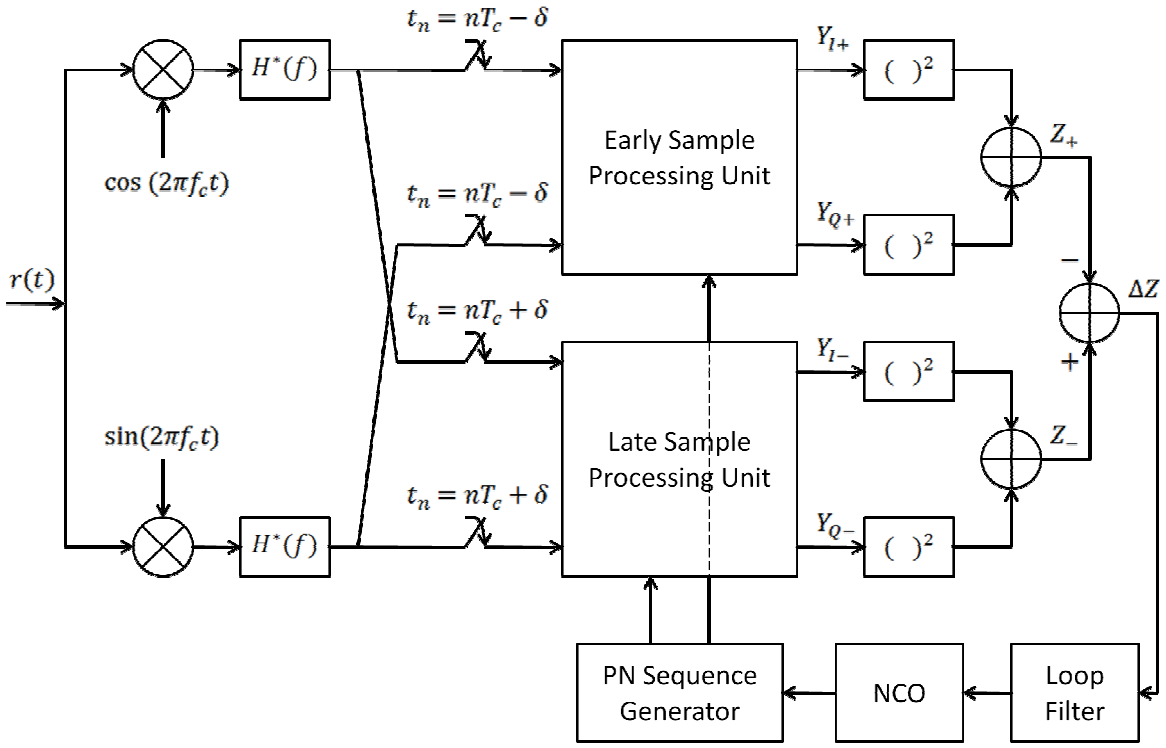

Figure 3-1: Processing Blocks of NC-DLL Tracking Loop

Figure 3.2 depicts a block diagram showing the different processing stages of a noncoherent DLL code tracking loop. In the figure, Y_{I-} and Y_{Q-} (or Y_{I+} and Y_{Q+}) represent the I- and Q-channel outputs of the early (or late) sample correlator. The sample correlator is depicted in Figure 3-3. K_0 and $\hat{\epsilon}$ are respectively the VCO gain and the estimated timing error. The I- and Q-channel input signals are oversampled usually eight times the PN chip rate. Early and late sample correlator outputs are used for generating the error signal ΔZ. After multiplication by the VCO gain, the error signal is low-pass filtered with a loop filter whose output corresponds to the timing error estimate. According to the timing error estimates, decimation points for the sample sequences are updated.

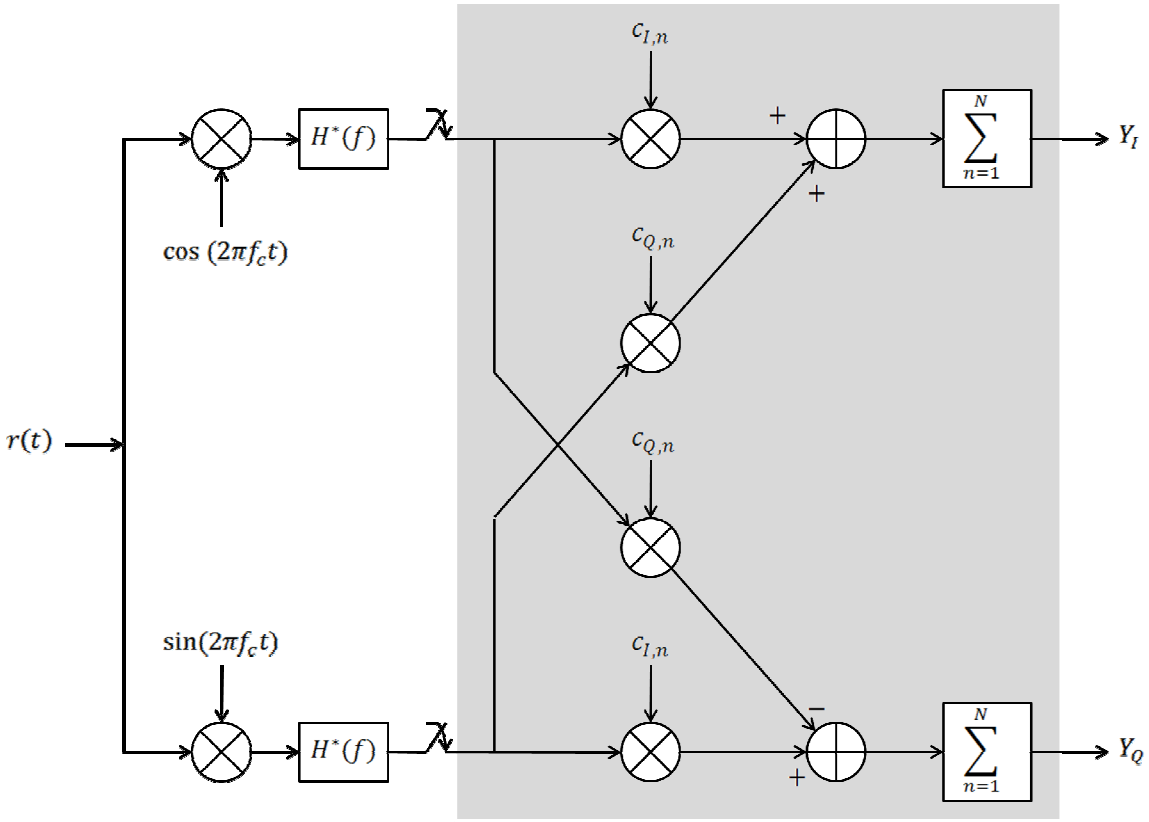

Figure 3-2: Early (late) sample correlator with QPSK spreading

When there is a timing error τ, the I- and Q-channel correlator outputs can be modeled as:

$$Y_I = AN\sqrt{E_c}R(\tau)\cos\varphi + n_I$$
$$Y_Q = AN\sqrt{E_c}R(\tau)\cos\varphi + n_Q \tag{3.9}$$

where A and φ are respectively signal envelope and phase, E_c is the signal energy per PN chip, and N is the number of accumulated PN chips. $R(\tau)$ is the convolution of the impulse responses of a pulse-shaping filter and its matched filter, given by

$$R(\tau) = h(\tau) * h(-\tau) = \int_{-\infty}^{\infty} |H(f)|^2 \cos(2\pi f_c \tau)\, df \tag{3.10}$$

where we have a root raised cosine pulse $h(\tau)$ with a 22% roll off factor. Computing the above integral by using the Fourier transform of $h(\tau)$ gives

$$R(\tau) = \frac{\cos(0.69115\,\tau)}{\pi\tau}\frac{\sin(\pi\tau)}{1-0.1936\tau^2} \tag{3.11}$$

The pulse-shaping filter is normalized so that $R(0) = 1$ without loss of generality. n_I and n_Q are the I- and Q-channel noise terms, each having a variance

$$E[n_I^2] = E[n_Q^2] = I_0/2 \tag{3.12}$$

where I_0 is the interference spectral density given by

$$I_0 = N_0 \int_{-\infty}^{\infty} |H(f)|^2 df \tag{3.13}$$

with N_0 denoting the power spectral densities of the background noise.

We can model the early sample and late sample correlator outputs for a flat-fading Rayleigh channel as follows [47]:

$$\begin{aligned} Y_{I\pm} &= AN\sqrt{E_c}R(\tau \pm \delta)\cos\varphi + n_{I\pm} \\ Y_{Q\pm} &= AN\sqrt{E_c}R(\tau \pm \delta)\cos\varphi + n_{Q\pm} \end{aligned} \tag{3.14}$$

with δ denoting a timing offset. Therefore, we can obtain

$$\begin{aligned} Z_- &= Y_{I-}^2 + Y_{Q-}^2 \\ &= A^2\left[N^2E_cR^2(\tau-\delta) + 2N\sqrt{E_c}R(\tau-\delta)(\cos\varphi\, n_{I-} + \sin\varphi\, n_{Q-})\right] + n_{I-}^2 + n_{Q-}^2 \end{aligned} \tag{3.15}$$

Similarly, Z_+ is

$$
\begin{aligned}
Z_+ &= Y_{I+}^2 + Y_{Q+}^2 \\
&= A^2\left[N^2 E_c R^2(\tau+\delta) + 2N\sqrt{E_c}R(\tau+\delta)(\cos\varphi\, n_{I+} + \sin\varphi\, n_{Q+})\right] + n_{I+}^2 + n_{Q+}^2
\end{aligned} \tag{3.16}
$$

The discriminator output thus becomes

$$
\begin{aligned}
\Delta Z &= Z_- - Z_+ \\
&= \beta A_k^2 \Bigg[N^2 E_c \Bigg(R^2\Bigg(\underbrace{\frac{\tau_k - \hat{\tau}_k}{T_c}}_{\epsilon_k} - \delta\Bigg) - R^2\left(\frac{\tau_k - \hat{\tau}_k}{T_c} + \delta\right)\Bigg) \\
&\qquad + 2N\sqrt{E_c}\Bigg(R\left(\frac{\tau_k - \hat{\tau}_k}{T_c} - \delta\right)(\cos\varphi\, n_{I-} + \sin\varphi\, n_{Q-}) \\
&\qquad - R\left(\frac{\tau_k - \hat{\tau}_k}{T_c} + \delta\right)(\cos\varphi\, n_{I+} + \sin\varphi\, n_{Q+})\Bigg)\Bigg] \\
&\qquad + n_{I-}^2 + n_{Q-}^2 - n_{I+}^2 - n_{Q+}^2
\end{aligned} \tag{3.17}
$$

This gives a convenient expression for the discriminator output ΔZ (we have discretized the equation 3.16 and normalized the timing error to within a chip interval):

$$
\begin{aligned}
\eta_k = \Delta Z_k &= \beta A_k^2 \Big(N^2 E_c \Big(R^2(\epsilon_k - \delta) - R^2(\epsilon_k + \delta)\Big)\Big) \\
&\qquad + 2N\sqrt{E_c}\big(R(\epsilon_k - \delta)\big(\cos\varphi\, n_{I-} + \sin\varphi\, n_{Q-}\big) - R(\epsilon_k + \delta)(\cos\varphi\, n_{I+} \\
&\qquad + \sin\varphi\, n_{Q+})\big) + \underbrace{n_{I-}^2 + n_{Q-}^2 - n_{I+}^2 - n_{Q+}^2}_{N_k} \\
&= \beta A_k^2 S(\epsilon_k) + N_k
\end{aligned} \tag{3.18}
$$

A_k is a Rayleigh random variable. N_k is the total sampled noise and includes the effects of thermal as well as interference from the same and adjacent cells of the mobile network. The factor β is a

power reduction factor (less than one) and is related to the cellular system environment. $S(\epsilon_k)$ is the S-curve for the loop, and $\epsilon_k = (\tau_k - \hat{\tau}_k)/T_C$ is the normalized tracking error in the interval $t_k \leq t < t_{k+1}$. A_k and N_k are mutually independent.

3.3 DLL in the Rayleigh fading environment

Let $h(k)$ be the impulse response of the digital loop filter, and let the gain of the numerically controlled oscillator (NCO) be denoted by K_{NCO}. Then, we can obtain the loop timing estimate

$$\frac{\hat{\tau}_k}{T_C} = \frac{\hat{\tau}_{k-1}}{T_C} + K_{NCO}\left[h(k-1) * \eta_{k-1}\right] \qquad t_k \leq t < t_{k+1} \tag{3.19}$$

Since $\frac{\hat{\tau}_k}{T_C} = \frac{\tau_k}{T_C} - \epsilon_k$, the normalized timing error ϵ_k in the interval $t_k \leq t < t_{k+1}$ can be expressed as

$$\epsilon_k = \epsilon_{k-1} + \frac{\tau_k}{T_C} - \frac{\tau_{k-1}}{T_C} - K_{NCO}\left(h(k-1) * \beta A_{k-1}^2 S(\epsilon_{k-1}) + N_{k-1}\right) \tag{3.20}$$

Since we are considering slowly time varying channels, $\tau_k \approx \tau_{k-1}$ and equations 3.21 becomes

$$\epsilon_k = \epsilon_{k-1} - K_{NCO}\left(\beta A_{k-1}^2 S(\epsilon_{k-1}) + N_{k-1}\right) \tag{3.21}$$

To facilitate theoretical analysis, we model the noise N_k as Gaussian and the timing error as a discrete-time continuous variable Markov process. The probability law of a discrete-time Markov process is completely characterized by the one-step transition probabilities $f_k(x'|x), x', x \in S'$ and the first order density $p_0(x), x \in S'$ where S' is the total state space [48]. The PDF of ϵ_k, conditioned on the initial timing error, satisfies the Kolmogorov-Chapman equation,

$$p_k(\epsilon|\epsilon_0) = \int_{-\infty}^{\infty} f_{k-1}(\epsilon|x)\, p_{k-1}(x|\epsilon_0) dx \tag{3.22}$$

where ϵ_0 is the initial timing error value, $p_k(\cdot\,|\epsilon_0)$ is the pdf of ϵ_k given ϵ_0 , and $f_{k-1}(\cdot\,|x)$ is the transition PDF of ϵ_k given $\epsilon_{k-1} = x$.

Since A_k^2 and N_{k-1} are independent, the transition pdf $f_{k-1}(\epsilon|x)$ can be derived by using the fact that ϵ_k is a function of two independent random variables A_k^2 and N_{k-1} as

$$\epsilon_k = x - K_{NCO}\Delta t\left(\beta A_{k-1}^2 S(\epsilon_{k-1}) + N_{k-1}\right) \tag{3.23}$$

Let $z \triangleq x - K_{NCO}\Delta t N_{k-1}$, then z will be a Gaussian random variable with mean x and variance $(K_{NCO}\Delta t\sigma_n)^2$ where σ_n^2 is the variance of N_{k-1}. From 3.20 we can calculate σ_n^2 as

$$\begin{aligned}\sigma_n^2 = E\Big[\Big(2N\sqrt{E_c}\big(R(\epsilon_k-\delta)\big(\cos\varphi\, n_{I-} + \sin\varphi\, n_{Q-}\big)\\ - R(\epsilon_k+\delta)\times(\cos\varphi\, n_{I+} + \sin\varphi\, n_{Q+})\big)\Big)^2\Big] + E\left[\left(n_{I-}^2 + n_{Q-}^2 - n_{I+}^2 - n_{Q+}^2\right)^2\right]\end{aligned} \tag{3.24}$$

With some mathematical manipulation we can obtain

$$\begin{aligned}\sigma_n^2 = {} & 2N^3 I_0 E_{c,p}\{R^2(\epsilon_k-\delta) - R^2(\epsilon_k+\delta)\}\\ & - 4N^3 E_{c,p} R(\epsilon_k-\delta)R(\epsilon_k+\delta)\{N_0 R(2\delta) + \rho_0 R_0(2\delta)\}\\ & + 2N^2 I_0^2 - 2N^2\{N_0 R(2\delta) + \rho_0 R_0(2\delta)\}^2\end{aligned} \tag{3.25}$$

where

$$R_0(\tau) = \frac{1}{T_C}\int_{-\infty}^{\infty} |H(f)|^4 \cos(2\pi f_c \tau)\, d\tau \tag{3.26}$$

To make our analysis tractable, we approximate the pulse-shaping filter to the ideal lowpass filter with $H(f) = 1/\sqrt{W}$ for $-W/2 \le f < W/2$ and $W = 1/T_C$. In this case $R(\tau) = R_0(\tau) = \mathrm{sinc}(\tau/T_C)$ and the variance σ_n^2 is given by

$$\begin{aligned}\sigma_n^2 &= 2N^2 I_0^2\{1 - R^2(2\delta)\} + 2N^3 I_0 E_c \\ &\quad \times \{R^2(\epsilon_k - \delta) - R^2(\epsilon_k + \delta) - 2R(\epsilon_k - \delta)R(\epsilon_k + \delta)R(2\delta)\}\end{aligned} \tag{3.27}$$

With the assumption that the timing error is small, that is $\epsilon_k \approx 0$, the variance becomes:

$$\sigma_n^2 = 2N^2 I_0^2\{1 - R^2(2\delta)\} + 4N^3 I_0 E_c R^2(\delta)\{1 - 2R(2\delta)\} \tag{3.28}$$

Having calculated the variance of N_{k-1} we consider the PDF of $z \triangleq x - K_{NCO}\Delta t N_{k-1}$

$$\begin{aligned}f_z(z) &= \frac{1}{\sqrt{2\pi}K_{NCO}\Delta t\sigma_n}\exp\left[-\frac{(z-x)^2}{2(K_{NCO}\Delta t\sigma_n)^2}\right] \\ &= \frac{1}{\sqrt{2\pi}K_2\sigma_n}\exp\left[-\frac{(z-x)^2}{2(K_2\sigma_n)^2}\right]\end{aligned} \tag{3.29}$$

where $K_2 \triangleq K_{NCO}\Delta t$.

Since the PDF of A_{k-1}^2 is exponentially distributed, and letting $v \triangleq -K_{NCO}\Delta t\beta S(x)A_{k-1}^2$, the PDF of v can be shown to be, when $S(x)$ is positive,

$$f_v(v) = \begin{cases}\dfrac{1}{K_1 S(x)}\exp\left[\dfrac{v}{K_1 S(x)}\right] & \text{for } v < 0 \\ 0 & \text{elsewhere}\end{cases} \tag{3.30}$$

where $K_1 = \beta P K_{NCO}\Delta t$ and $P = E\left[A_{k-1}^2\right]$ is the average signal power. If $S(x)$ is negative, the PDF of v is given by

$$f_v(v) = \begin{cases} \dfrac{-1}{K_1 S(x)} \exp\left[\dfrac{v}{K_1 S(x)}\right] & \text{for } v > 0 \\ 0 & \text{elsewhere} \end{cases} \tag{3.31}$$

The transition PDF can be obtained as the convolution of the PDFs of s and v:

$$\begin{aligned} f_{k-1}(\epsilon|x) &= \int_{-\infty}^{\infty} f_z(\epsilon - v)\, f_v(v) \\ &= \begin{cases} \dfrac{1}{K_1 S(x)} \exp\,(\Gamma_1) \cdot Q(\Lambda_1) & \text{if } S(x) > 0 \\ \dfrac{-1}{K_1 S(x)} \exp\,(\Gamma_1) \cdot Q(-\Lambda_1) & \text{if } S(x) < 0 \\ \dfrac{1}{\sqrt{2\pi} K_2 \sigma_n} \exp\left[-\dfrac{(z-x)^2}{2(K_2\sigma_n)^2}\right] & \text{if } S(x) = 0 \end{cases} \end{aligned} \tag{3.32}$$

where

$$Q(y) \triangleq \frac{1}{\sqrt{2\pi}} \int_y^{\infty} \exp\left(\frac{-x^2}{2}\right) dx$$

$$\Gamma_1 = \frac{K_2^2 \sigma_n^2}{2K_1^2 S^2(x)} + \frac{\epsilon - x}{K_1 S(x)}$$

$$\Lambda_1 = \frac{\epsilon - x + \dfrac{K_2^2 \sigma_n^2}{K_1 S(x)}}{K_2 \sigma_n}$$

It can be observed that $f_{k-1}(\epsilon|x)$ is independent of k. The PDF of the normalized tracking error, $p(\epsilon|\epsilon_0)$ can now be calculated by iterating the Kolmogorov-Chapman equation in 3.25.

3.4 DLL in the Rician fading environment

As discussed before, for line-of-sight (LOS) conditions the first arriving path is Rice distributed. For a flat-fading Rician channel, the same analysis as before applies, with the exception that A_{k-1} in 3.24 has a Rician distribution, given by

$$p(A_k) = \frac{A_k}{\sigma_n^2} \exp\left(-\frac{A_k^2 + C^2}{2\sigma_n^2}\right) I_0\left(\frac{A_k C}{\sigma_n^2}\right), \quad A_k \geq 0 \tag{3.33}$$

Here $I_0(\cdot)$ is the modified Bessel function of the first kind and order zero. $2\sigma_n^2 + C^2$ is the total signal power in the first path, with C^2 the power of the specular component and $2\sigma_n^2$ the power of diffuse component. It may be noted that for a Rician distributed A_k, v in 3.33 is no longer exponentially distributed. The distribution of v in this case is easily calculated as (for negative v; the case for positive v is similar)

$$f_v(v) = \begin{cases} \frac{1}{2\sigma_n^2} \frac{1}{K_1 S(x)} \exp\left[\frac{1}{2\sigma_n^2}\left(\frac{v}{K_1 S(x)} - C^2\right)\right] I_0\left(\frac{A\sqrt{\frac{-v}{K_1 S(x)}}}{\sigma_n^2}\right) & \text{for } v < 0 \\ 0 & \text{elsewhere} \end{cases} \tag{3.34}$$

The convolution in 3.32, however, cannot be found in closed form for the Rician case. Therefore, it is computed numerically by using Mathematica's built-in routines for numerical integration.

3.5 Numerical Results

We now present different numerical results to illustrate the DLL performance analysis discussed above. The following power delay profile is considered for a three-component discrete multipath frequency selective channel. The DLL attempts to track the earliest path at delay τ_0.

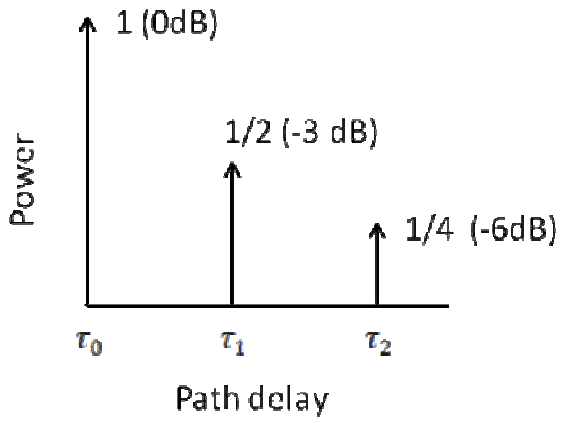

Figure 3-3 Multipath Intensity Profile for Rayleigh Fading Channel

The basic technique that is employed to get these stationary PDFs is iterating the Kolmogorov-Chapman equation given in 3.22. We iterate the equation from $k = 0,1, \ldots$ until the PDF function $p_k(\epsilon|\epsilon_0)$ stops changing appreciably. For the initial distribution at the zeroth iteration, we have $p_0(\epsilon|\epsilon_0) = \delta(\epsilon - \epsilon_0) = \delta(\epsilon)$, (taking $\epsilon_0 = 0$). Successive PDFs $p_k(\epsilon|\epsilon_0)$ are computed by performing the numerical integration given in equation 3.22. The information needed for this operation is the transition PDF $f_k(\epsilon|\epsilon_{k-1})$, which is the conditional distribution of ϵ_k given ϵ_{k-1}. For this purpose, we use equation 3.21 that describes the overall system. $f_k(\epsilon|\epsilon_{k-1})$ is then a sum of an independent Gaussian and a Rayleigh random variable. It is possible to obtain a closed form expression for the transition PDF by computing the convolution of the PDF expressions for Gaussian and Rayleigh random variables. However, when considering Rician fading, no closed form expression for $f_k(\epsilon|\epsilon_{k-1})$ can be obtained. In this case, convolution is performed numerically. In the absence of the detailed modeling of multipath, multi-user fading channel, it is customary to assume that the tracking error PDF is normal distributed. In the following, three different cases (for different number of users in the system) are considered. Although the Gaussian approximation may be good when the number of users is low, it becomes less and less accurate as the number of users increase and as the SNR is decreased for a high number of users.

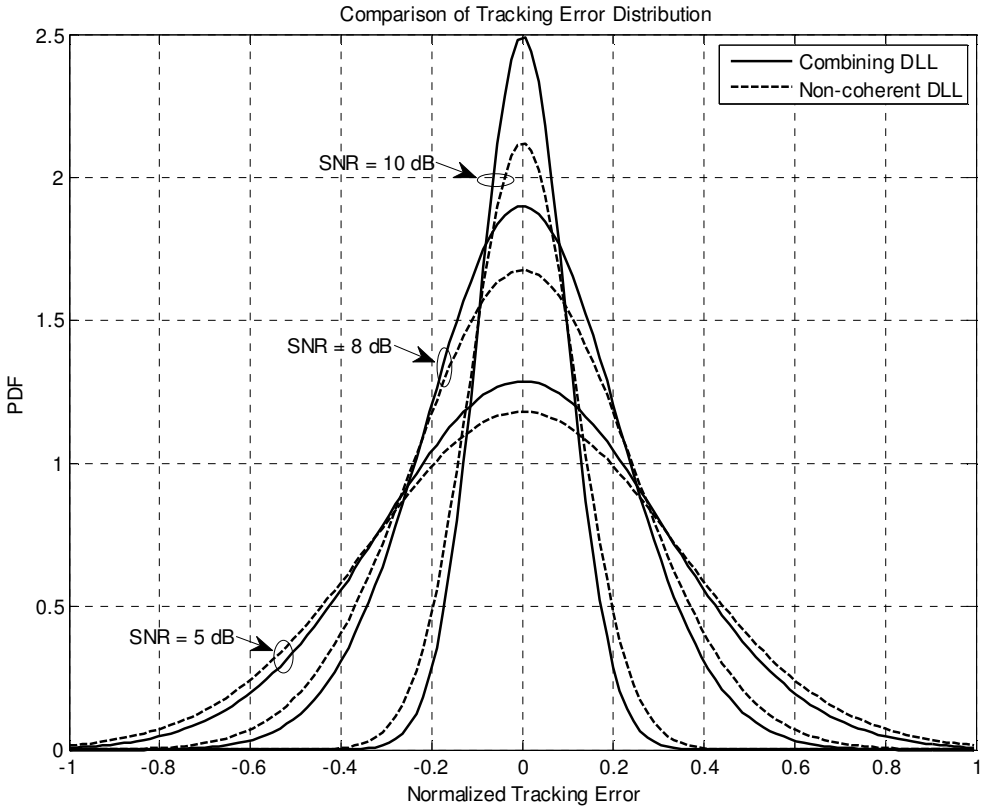

Figure 3-4: Comparison of Tracking Error PDFs for Combining and Non-coherent DLL under Rayleigh Fading with early-late offset of 0.5

Figure 3-4 compares the PDFs of the normalized tracking error for the NC-DLL and the RAKE-like combining DLL under Rayleigh fading conditions for SNRs of 5 dB, 8 dB and 10 dB. The ratio of power in the first path to the power in the second path is 3 dB. We see that the NC-DLL, just like the coherent non-combining DLL, has a lower tracking error performance than that of the RAKE-like combining DLL at all values of SNR. Furthermore, the difference in performance is greater than that with the coherent DLL (compared to Figure 2-5 the difference in PDF peaks is greater in Figure 3-4). The performance difference is more pronounced at higher SNRs.

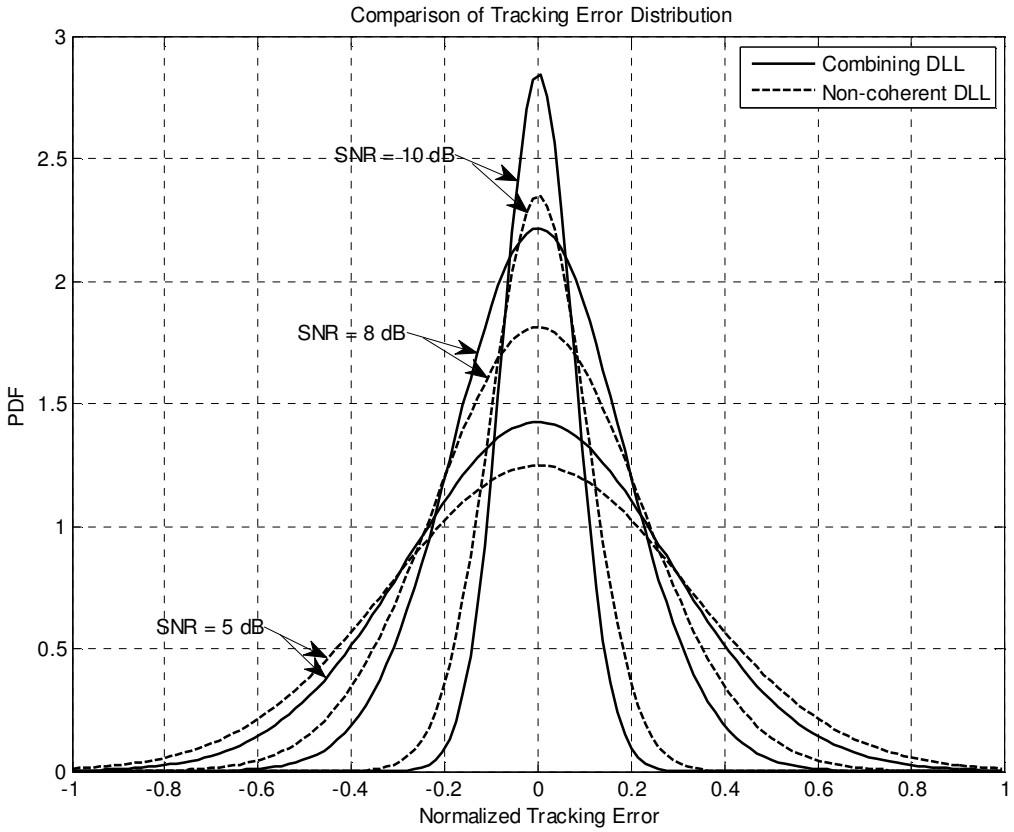

Figure 3-5: Comparison of Tracking Error PDFs for Combining and Non-coherent DLL under Rician Fading with early-late offset of 0.5 and a Rice factor of 5

Figure 3-5 compares the PDFs of the normalized tracking error for the NC-DLL and the RAKE-like combining DLL under Rician fading conditions for SNRs of 5 dB, 8 dB and 10 dB. A Rice factor of 5 was used for the calculation of the PDFs. Again, we see that the NC-DLL has a lower tracking error performance than that of the RAKE-like combining DLL. In Figure 3-5, the difference between PDF peaks is even more pronounced than that in Figure 3-4 (Rayleigh fading).

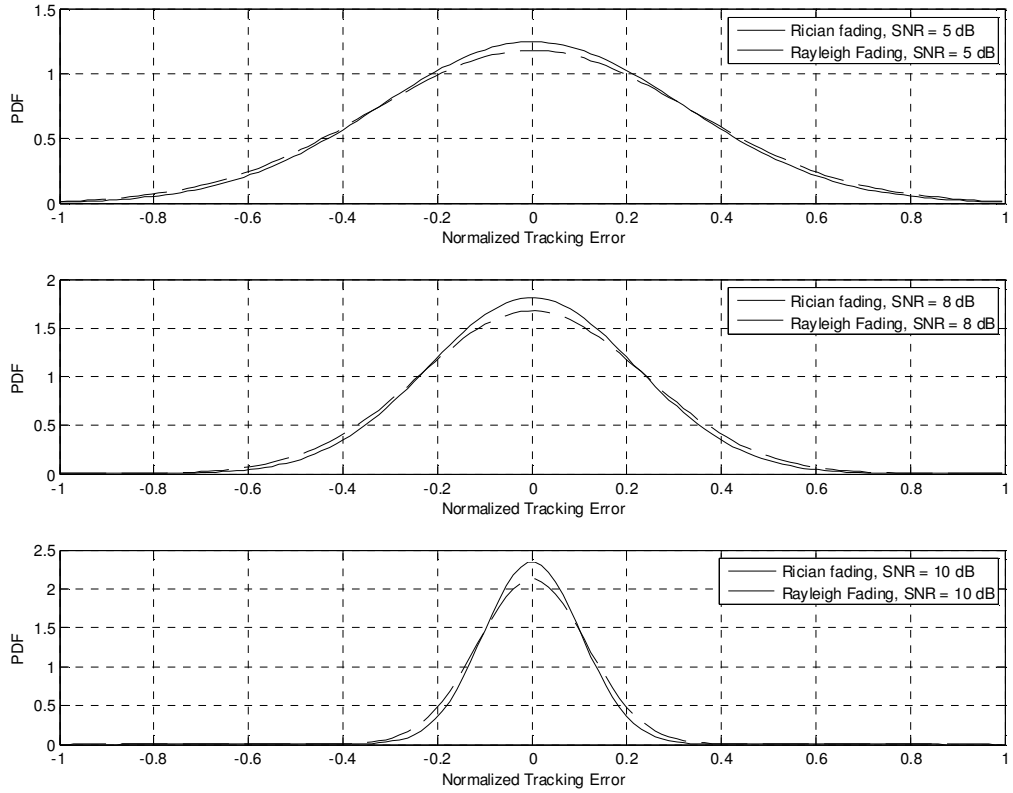

Figure3-6: Comparison of tracking error PDFs for the non-coherent DLL under Rayleigh and Rician fading, with an early late offset of 0.5 and a Rice factor of 5

Figure 3-6 gives a comparison of the PDFs of normalized tracking error for the NC-DLL under Rayleigh and Rician fading. The SNRs used for the calculation of PDFs are 5 dB, 8 dB and 10 dB. As with the combining DLL, we see that in the case of Rician fading the PDF has a lower variance than that in for Rayleigh fading. Also as the SNR increases the difference between the peaks of the PDF for the two cases increases. The early-late offset is 0.5 and the Rice factor used for the calculation of the PDFs is 5.

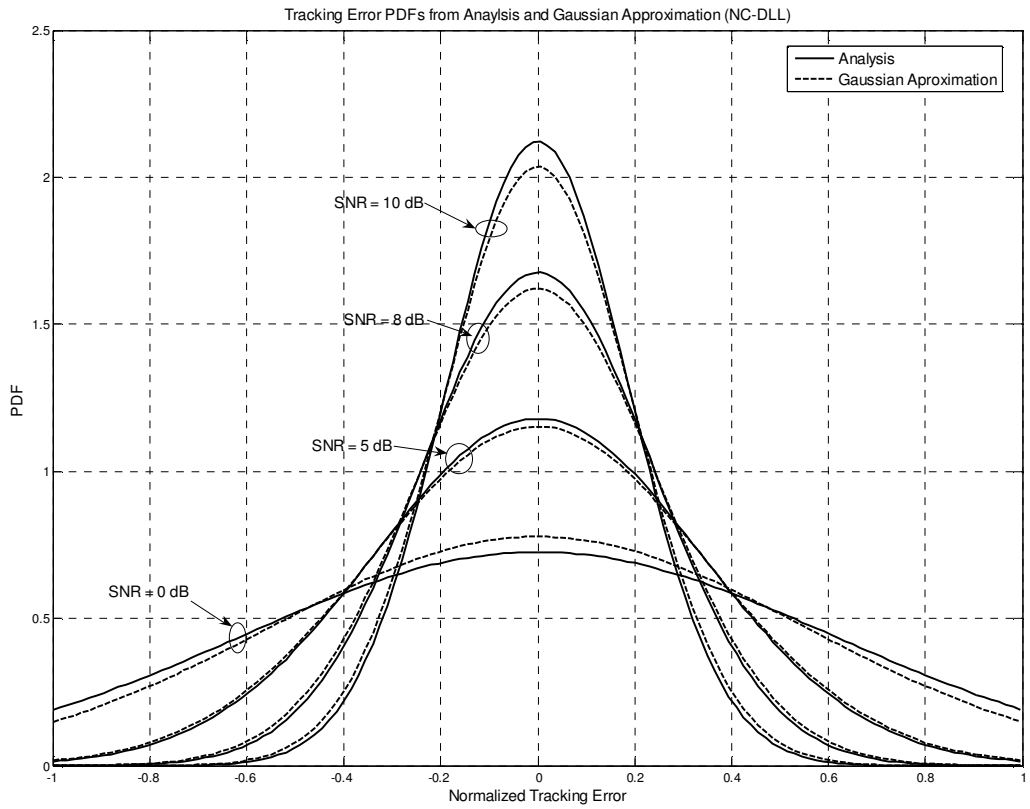

Figure 3-7: Comparison of tracking error PDFs from analysis and Gaussian approximation for the NC-DLL (Rayleigh Fading, early-late offset of 0.5)

Figure 3-7: compares the PDFs of the normalized tracking error for NC-DLL and the corresponding Gaussian approximations under Rayleigh fading conditions for SNRs of 0 dB, 5 dB, 8 dB and 10 dB. The ratio of power in the first path to the power in the second path is 3 dB. It is seen that the Gaussian approximation gives pessimistic results for high SNRS (> 0 dB), while at low SNRs (0 dB) the Gaussian approximation gives optimistic results. This trend was also seen in the comparison of true PDF of the RAKE-DLL and the corresponding Gaussian approximation.

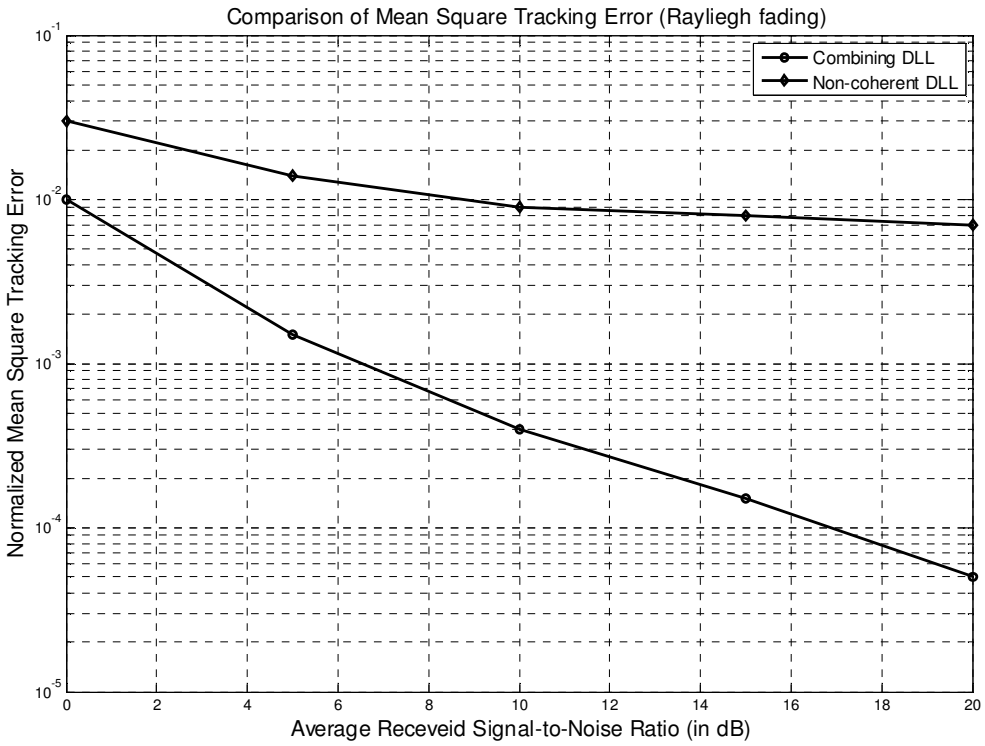

Figure 3-8: Comparison of Mean Square Tracking Error for the non-coherent DLL and combining DLL under Rayleigh fading

Figure 3-8 compares the variance of the normalized tracking error for the NC-DLL and the combining DLL, under Rayleigh fading conditions. The power ratio of the first path to the second path is 3 dB. We see that the combining DLL outperforms the NC-DLL at all values of SNR. At low SNRs the performance difference between the two DLLs is relatively small, but at high SNRs a performance floor emerges for the non-combining DLL while the combining DLL shows a continuous decrease in mean square tracking with the increase in SNR.

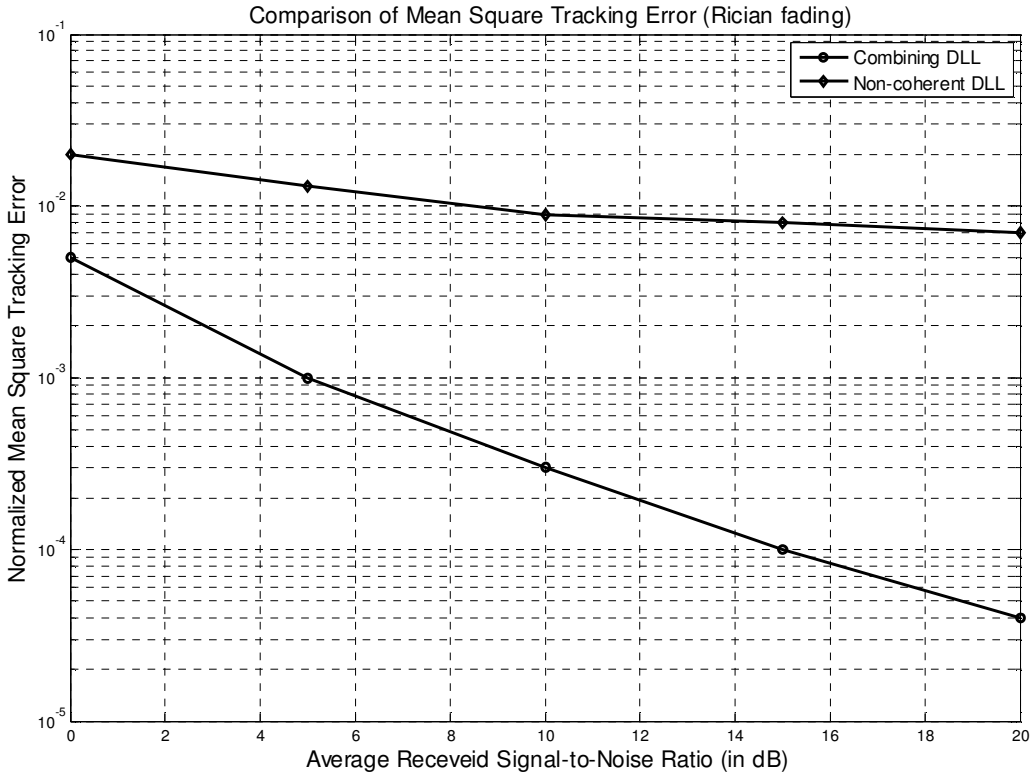

Figure 3-9: Comparison of Mean Square Tracking Error for the non-coherent DLL and combining DLL under Rician fading (Rice Factor of 5)

Figure 3-9 compares the variance of the normalized tracking error for the NC-DLL and the combining DLL, under Rician fading conditions. The Rice factor used for the calculation of the mean square tracking error is 5. As in Figure 3-7, we see that the combining DLL outperforms the NC-DLL. Again, at low SNRs the performance difference between the two DLLs is relatively small, but at high SNRs a performance gap increases by several orders of magnitude. The performance floor for the NC-DLL persists at high SNRs under Rician fading.

3.6 Summary and Conclusion

The probability distribution for the normalized tracking error of the non-coherent digital DLL was obtained. The system model we considered took into account quadrature spreading and multipath fading. The DLL discriminator output was expressed as a function of the S-curve of the loop. A Stochastic Difference Equation (SDE) that describes the dynamics of the discrete time tracking error process was developed for the Rayleigh/Rician fading channel. The SDE that describes the tracking error process showed that the process is first-order Markovian. A closed-form expression for the transition PDF of this Markov process was obtained. The steady state PDF of the tracking error was computed using an initial PDF, the computed transition PDF and by iterating the Kolmogorov-Chapman equation of the Markov process several times. The PDF results were compared with that of combining DLL from Chapter 2. The combining DLL clearly outperforms the non-coherent DLL at all SNR values. However, in terms of implementation complexity, the non-coherent DLL is more practical.

Chapter 4 Application to ToA Location in CMDA Cellular Networks

4.1 Introduction

As discussed in Chapter 1, wireless mobile communication systems have experienced a tremendous growth. A rich set of features in addition to basic phone services are now becoming available. Among these features are radiolocation services through which the mobile station's position can be determined by combining information from different base stations that are in radio link with the mobile station in question. Many services can be supported through this positioning capability including medical emergency, law enforcement, location-specific commercial advertisement and network provisioning and optimization based on subscribers' geographical distribution throughout the service area.

In CDMA systems, several techniques can be employed for network-based subscriber positioning. They are generally based on signal strength of arrival (SoA), time of arrival (ToA) or angle of arrival (AoA). In this chapter, we consider the ToA method since the information required for positioning is already available from the DLL used to track the incoming code. We apply the analysis of Chapter 3 to wireless positioning scenarios in a typical CDMA network setting. The performance of the positioning algorithms is degraded because of certain limitations imposed by the cellular environment, such as severe multipath and multiple-access interference (MAI) as discussed in Chapter 1. In the case of CDMA systems, MAI has special significance because power

control mechanisms are always operating to maintain the received power from different users at the same level at their respective serving base stations. However, at the other base stations which are co-locating the mobile, the mobile's received power can be very low compared to other users, and therefore its ToA estimation will be very noisy, which will in turn affect the accuracy of the mobile positioning algorithms. This effect of this problem of "hearability" has been taken into account in [49]. We also address this problem in the present chapter, and we show that radiolocation accuracy can vary considerably, depending on the mobile link quality with the base stations involved in its position determination. Our approach differs from that of [49] in two respects. First, we explicitly model the tracking error statistics for the DLL as opposed to relying on numerical simulations to obtain histograms for the PDFs of the tracking error. Second, the analysis in [49] assumes BPSK modulation for the spread spectrum signal, whereas our analysis assumes quadrature spread modulation following the 3G UMTS standard. It is shown that the near-far problem due to other-cell multiple-access interference, which cannot be mitigated by power control mechanisms, adversely affects the ability of the other non-serving base stations to correctly estimate the ToA of the intended mobile signal. This in turn leads to poor positioning capability, which requires correct timing estimation by the serving base station and at least two additional stations. Different scenarios are examined on the basis of the level of soft handoff connectivity of the mobile.

4.2 System Model

We employ the system model used in [49]. Consider a cellular network consisting of a central cell with two tiers of surrounding cells as illustrated in Figure 4-1. The arrangement is sufficient to accurately model interference statistics. Mobile stations are assumed to be uniformly distributed across the network coverage area. The signal propagating through the channel between the mobile (MS) and base station (BS) undergoes attenuation including distance path loss and log-normal

shadowing. Since CDMA systems employ power control mechanisms, at a given base station of interest termed as the "serving" base station, all mobiles are received with nearly the same power. However, not all base stations in the cellular environment receive the mobile signal at the same power level. At neighboring base stations, a given mobile served by the first base station can be received at much lower power compared to the mobiles belonging to that neighboring cell. Time-of-arrival estimation accuracy strongly depends on the received multiple-access interference (MAI) levels. This issue is of paramount importance in mobile radiolocation which typically requires ToA data from at least three base stations. We will use β in Equation 4-1 to model the reduction in received power at the "non-serving" base stations, i.e. base stations that belong to cells other than the one in which the user is located.

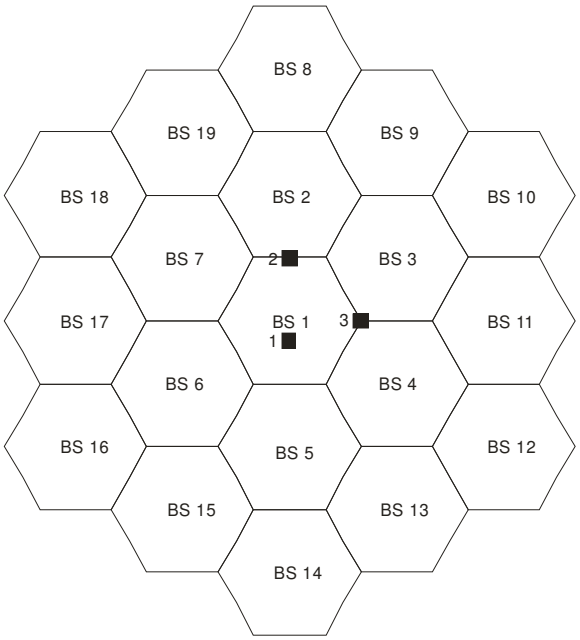

Figure 4-1: Typical layout of cells in a CDMA network. BS1 is serving, while all other BSs are interfering

We illustrate this cellular environment in Figure 4-1. The mobile is being served by the center base station BS 1. A minimum of three base stations, BS 1, BS 2 and BS 3 co-locate MS by using standard location ToA algorithms. As in [49], [50] we can define β_i as the ratio of average received power at BS *i* compared to BS 1:

$$\beta_i = \frac{P_i}{P_1} \tag{4.1}$$

This ratio can fluctuate widely, depending on the mobile position relative to the base stations of interest. Figure 4-1 gives an example of three different scenarios (cases 1, 2 and 3). Case 1 is where a mobile is in close proximity to its serving base station, BS 1, with a signal, for example, at 10dB above that at the other two base stations. Case 2 represents a two-way soft handover scenario, where the mobile power at base station 2 is within 3dB from that at BS 1. Case 3 denotes the 3-way soft handover situation where the mobile signal is within 3dB at both BS 2 and BS 3 compared to BS 1. By using different values of β to model these cases, we will obtain the timing error distribution at each of the locating base stations. This will enable an accurate performance analysis of the location algorithm in a realistic cellular environment.

4.3 Time of Arrival Estimation

As discussed in Chapter 1, timing synchronization for CDMA signals is typically implemented by a two-step process consisting of a coarse acquisition timing search to within a given uncertainty range on the order of one-chip interval, which is then followed by fine time tracking achieved by a delay-locked loop DLL mechanism which is described in detail in Chapter 3 (Figure 3-1). For each base station involved in mobile positioning, a DLL block continuously attempts to bring the local code timing estimate into perfect alignment with the incoming mobile signal. However, this timing

estimation will be subject to error due to noise, multipath fading and multiple-access interference. For frequency-selective fading environments, the total received signal at the DLL input can be expressed as:

$$r(t) = \frac{\beta}{2}\Re\mathrm{e}\left[\sum_{i=1}^{M}\sum_{k=-\infty}^{\infty} c_{k\ (mod\ N)}h(t - kT_c - \tau_i)a_i e^{j2\pi f_c t}\right] + n_T(t) \tag{4.2}$$

where β is the received signal power, $\{c_k\}$ is the complex spreading code sequence with a period N, $h(t)$ is the implies response of a pulse shaping filter (taken to be a root-raised cosine with 22% roll-off, as per 3G UMTS standard), T_c is the chip symbol duration, M is the number of resolvable multipath signals and a_i and τ_i are the i-th fading path gain and time delay. The signal $n_T(t)$ is a narrow band noise process, and it represents the total thermal and multiple access interference noise due to the same cell as well as other cell users.

In the following, we focus on estimating the TOA of the first arriving path with delay τ_o. As illustrated in Figure 3-1, we adopt a non-coherent DLL structure with two early-late branches. The received signal is correlated with code replicas $c\left(t-\hat{\tau}_o+\Delta\right)$ and $c\left(t-\hat{\tau}_o-\Delta\right)$, where $\hat{\tau}_o$ is the local code timing estimate. The outputs are envelope-detected, and the filtered difference is used to drive the voltage controlled oscillator (VCO) which controls the code timing adjustment. The DLL performance is dependent upon the discriminator output

$$\begin{aligned}\Delta Z_k = \beta A_k^2\Big(&N^2E_c\Big(R^2(\epsilon_k-\delta)-R^2(\epsilon_k+\delta)\Big)\Big)\\ &+2N\sqrt{E_c}\big(R(\epsilon_k-\delta)\big(\cos\varphi\, n_{I-}+\sin\varphi\, n_{Q-}\big)-R(\epsilon_k+\delta)(\cos\varphi\, n_{I+}\\ &+\sin\varphi\, n_{Q+})\big)\end{aligned} \tag{4.3}$$

where the code autocorrelation function is defined as $R(\tau) = 1/NT_c \int_0^{NT_c} c(t)c(t+\tau)dt$. The normalized S-curve is defined as:

$$S(\epsilon_k) = N^2 E_c\big(R^2(\epsilon_k - \delta) - R^2(\epsilon_k + \delta)\big) + 2N\sqrt{E_c}\big(R(\epsilon_k - \delta)\big(\cos\varphi\, n_{I-} + \sin\varphi\, n_{Q-}\big) - R(\epsilon_k + \delta)(\cos\varphi\, n_{I+} + \sin\varphi\, n_{Q+})\big) \quad (4.4)$$

where $\epsilon_k = \frac{\tau_k - \hat{\tau}_k}{T_c}$ is the normalized timing error, and $\delta = \Delta/T_c$ is the early-late discriminator offset. A common figure of merit for analyzing the DLL performance is the timing error variance (or rms jitter). The analysis based on the Kolmogorov-Chapman equation of the tracking error process is used to carry out a computation of the timing error variance. The full analysis is given in Chapter 3.

Due to the power control mechanisms, at a given base station of interest termed as the "serving" base station, all mobiles are received with nearly the same power. However, at the neighboring base stations, a given mobile served by the first base station can be received at much lower power compared to the mobiles belonging to that neighboring cell. The factor β appearing in 4-1 is related to the mobile cellular environment, and it can be substantially different for each of the base stations involved. Since time-of-arrival estimation accuracy strongly depends on the received multiple-access interference (MAI) levels, this issue is of paramount importance in mobile radiolocation which typically requires ToA data from at least three base stations. For our purpose, in the DLL performance results presented here, the β factors (defined as the ratio of average received power at BS i compared to BS 1) are used to model the reduction in received power at the "non-serving" base stations. These ratios can fluctuate widely, depending on the mobile position relative to the base stations of interest. Case 1 is where a mobile is in close proximity to its serving base station,

BS 1, with a signal, for example, at 10dB above that at the other two base stations. Case 2 represents a two-way soft handover scenario, where the mobile power at base station 2 is within 3dB from that at BS 1. Case 3 denotes the 3-way soft handover situation where the mobile signal is within 3dB at both BS 2 and BS 3 compared to BS 1. By using different values of β to model these cases, we obtain the timing error distribution at each of the locating base stations.

4.4 Numerical Results

In the following three figures, three different positioning scenarios in a cellular environment are considered. Case 1 refers to the case where the MS is close to the serving base station and there is no soft handoff with the neighboring cell base stations. Case 2 is where the MS is in on the edge of its serving cell and is in a soft handoff involving 2 BS (2-way handoff). Case 3 is where the MS is near the corner of its serving cell and is in a soft handoff involving its serving BS and 2 neighboring BS (3-way handoff). Power control mechanism employed in CDMA networks play a crucial role in the DLLs tracking performance at each of the base stations. For all users to be received with equal power in a given cell, those MS which are closer to the serving BS are required to power down. However, this causes that user's signal to be received with very low power at neighboring base stations that are involved in positioning through delay lock tracking of the user's PN signal. However, when the MS is in involved in a soft handoff, there is an improvement in tracking performance, as the results below indicate. It is to be noted that the PDFs of the normalized tracking error is non-zero on the interval [-1.5, 1.5]. This interval is exactly where the S-curve of the DLL is non-zero, given by Equation 3.18. The scale on the x-axis in the following figures goes from -0.5 to 0.5. This has been done for clarity, as the PDFs are narrower in some cases and have tails that lie approximately outside the interval [-0.5, -0.5]. In Figure 4-9, however, the x-axis covers the full interval [-1.5, 1.5] as the PDFs are broader.

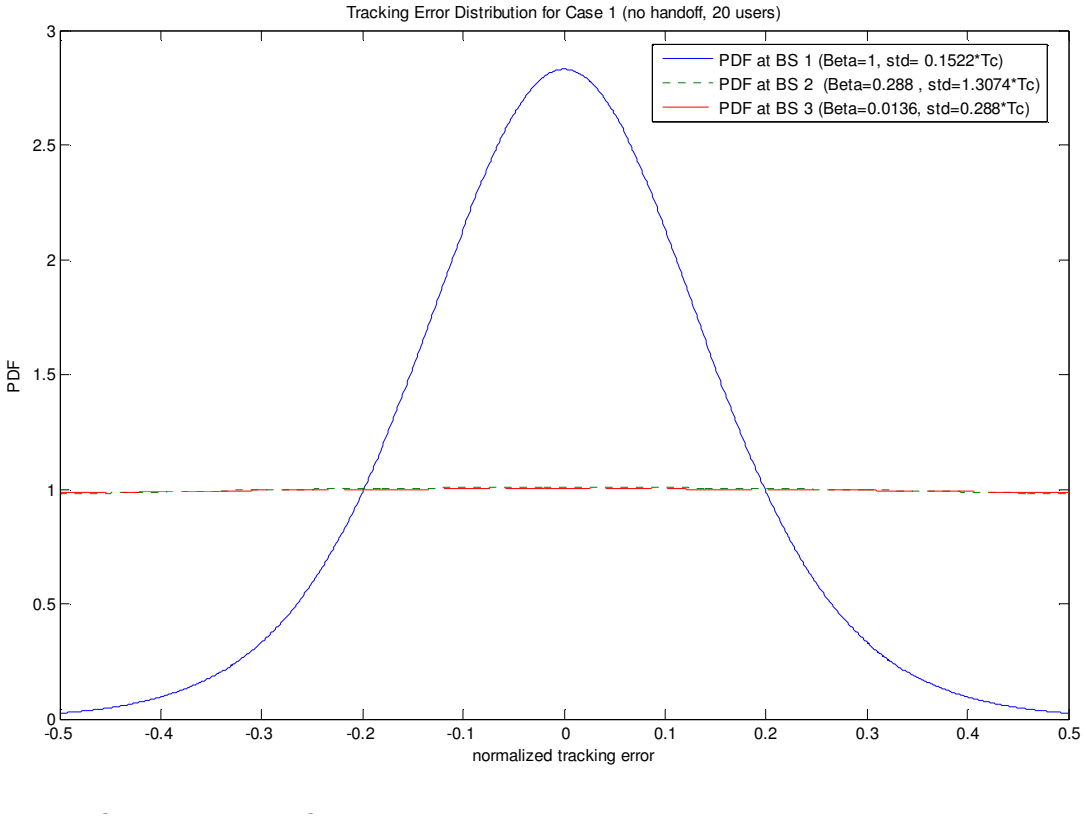

Figure 4-2 draws a comparison of the tracking error distribution for Case 1 (no handoff). It can be seen that because of power control mechanisms, the base stations in cell 2 and cell 3 (neighboring cells of cell 1) show a very poor tracking performance. The tracking error PDF at BS 2 and BS 3 is almost uniform while the PDF observed at BS 1 has a high curvature, allowing better estimation accuracy of the PN signal delay.

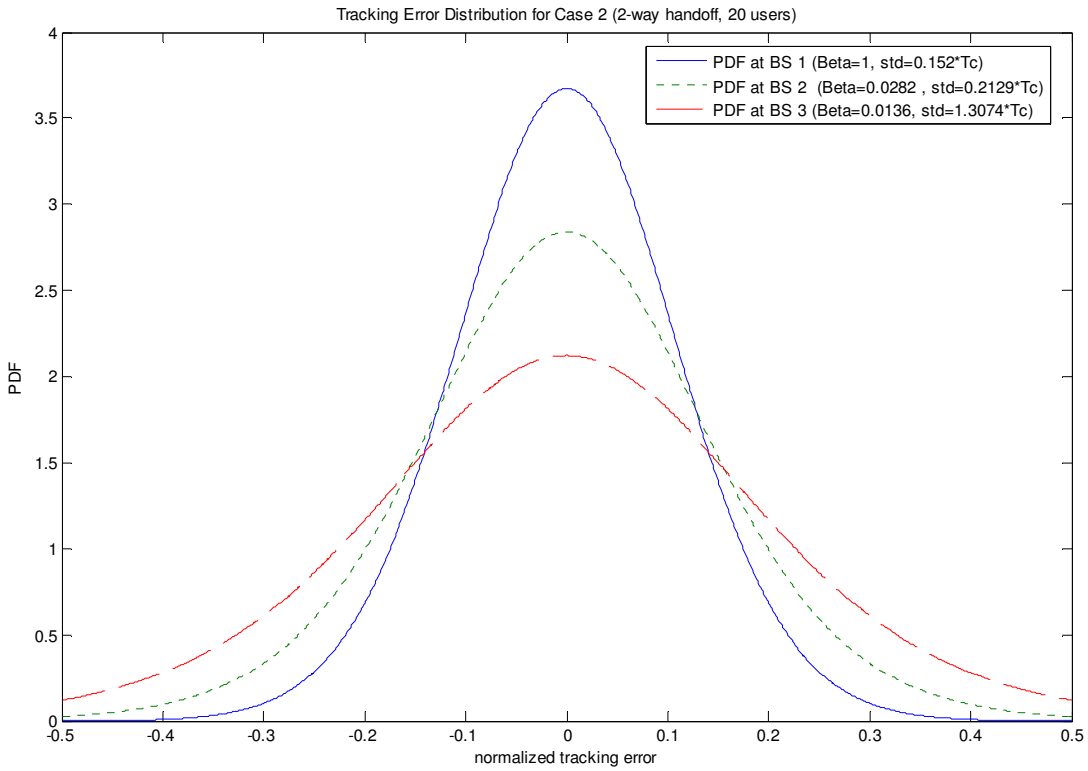

Figure 4-3: Tracking error PDF at BS1, BS2, BS3 for MS in 2-way soft handoff, (case 2)

Figure 4-3: the case of 2-way handoff is considered. Here the tracking accuracy at BS 2 and BS 3 has increased, because the MS is received at these base stations at a higher power.

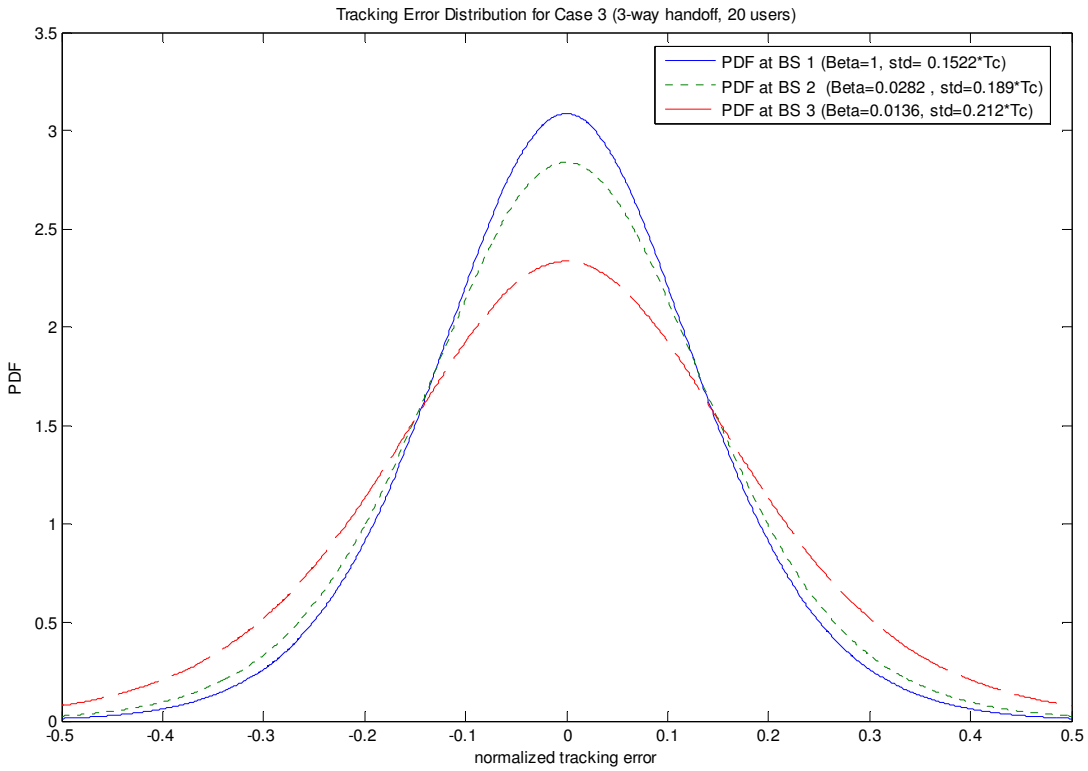

Figure 4-4: Tracking error PDF at BS1, BS2, BS3 for MS in 3-way soft handoff, (case 3)

Figure 4-4 is the final positioning scenario (case 3) where 3 base stations are involved in a soft handoff. It is apparent that the tracking accuracy at BS 2 and BS 3 has substantially improved relative to the previous cases. In fact, the tracking error PDF at BS 2 approaches the distribution at BS 1 closely. The widely varying tracking performance at the three BS involved in position of the MS for the three different cases needs to be taken into account when considering the performance of any location algorithm.

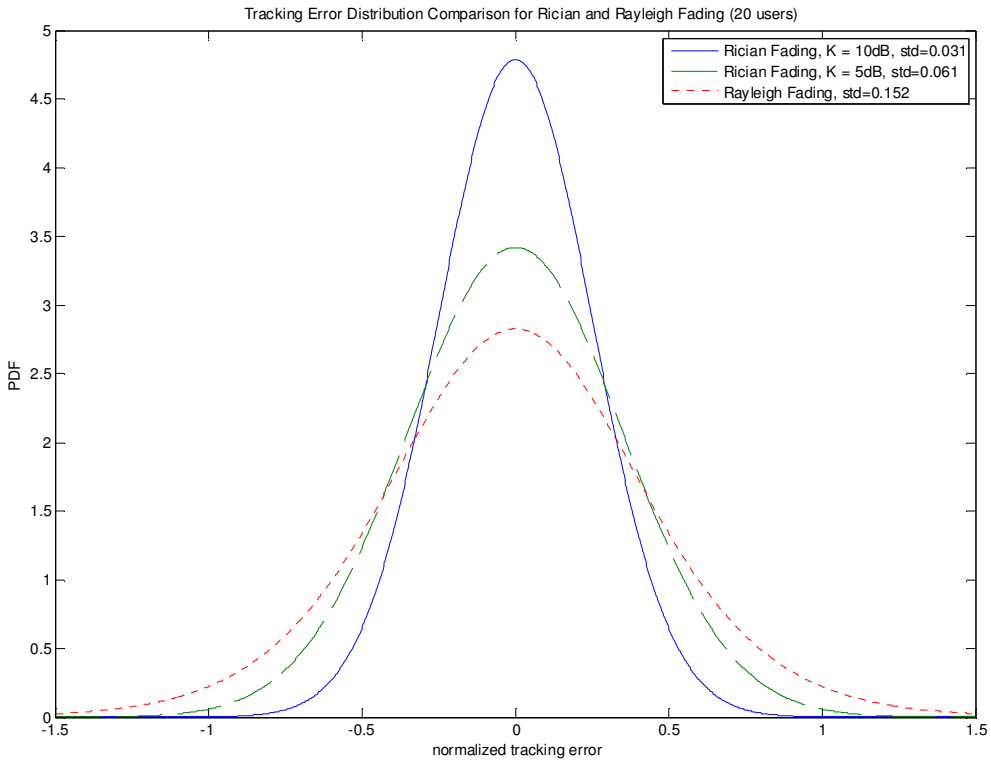

Figure 4-5: Tracking error PDFs for LOS and NLOS positioning Scenarios

Figure 4-5 takes into account LOS and NLOS conditions. For line-of-sight signal propagation between the MS and BS (a direct path between the two), the fading statistics are Rician, while for NLOS conditions the fading is Rayleigh distributed. Figure 4-9 shows the loss in tracking performance that is incurred for NLOS conditions relative to LOS propagation with a Rice factor of 5dB and 10dB.

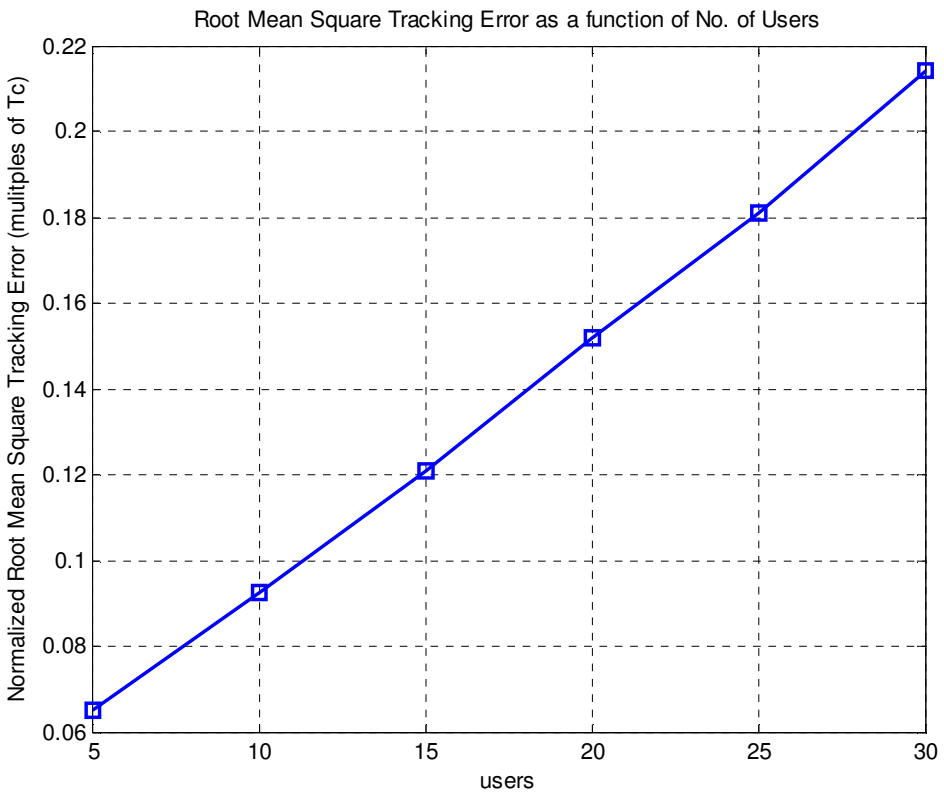

Figure 4-6: Effect of Users on RMS Tracking Error

In Figure 4-6, the root mean square tracking error (standard deviation of the tracking error PDF) versus the number of users in the system is plotted. It seems that more or less, the RMS error tracking error increases linearly with the number of users.

4.5 Summary and Conclusion

In this chapter, the tracking error performance for the DLL was obtained in a typical cellular environment. Performance evaluation was done by comparing the probability distributions of the tracking error MS located at different positions in a cell. The tracking error statistics directly affect the performance of ToA based positioning algorithms in CDMA networks. Three scenarios were

considered. In Case 1, the MS is located very close to its serving BS and is not in handoff with any other BS. In Case 2, the MS is on the edge of its serving cell and is in a soft-handoff involving one more BS. In Case 3, the MS is near the corner of its serving cell and is in a soft-handoff involving its serving BS and 2 neighboring BS. It was seen that DLL performance, in terms of the PDF of the tracking error, improves as the number of hand-offs increase. Mean square tracking error was also plotted as a function of the number of users in a cell. It was observed that the mean squared tracking error increases linearly with the number of users. Finally, it was shown that DLL performance was better under LOS signal propagation conditions than under NLOS propagation.

Chapter 5 Conclusion and Recommendations for Future Work

5.1 Summary and Conclusions

In this thesis, we investigated the performance of code tracking loops for CDMA signals under realistic channel conditions that include multipath fading and multiple access interference. The statistics for the residual tracking error were obtained through analytical derivations. The importance of these statistics is twofold. First, they characterize the performance of the synchronization system of the receiver. Synchronization is critical to CDMA receiver performance. Secondly, these statistics give the accuracy of the time-of-arrival (ToA) measurement made by using delay lock loops for wireless positioning in a cellular environment.

In Chapter 2, we presented an analysis of the first-order statistics for the RAKE-like combining DLL. In contrast to the traditional approach of linearizing the loop equation for the DLL, our formulation considered the full non-linear model for the DLLs. The PDF for the combining DLL was obtained by solving the Fokker-Plank equation associated with the stochastic differential equation of the DLL. The Fokker-Plank method can be applied only to continuous time stochastic processes. As the RAKE-DLL we considered was analog, its tracking error process was continuous time. The Fokker-Plank method could thus be fruitfully applied. The PDF for the RAKE-DLL was obtained through numerical integration of a four-dimensional integral. The combining DLL was compared with the traditional coherent DLL. It was found that the combining DLL outperforms the

traditional DLL at all SNRs. The PDFs were computed for both Rayleigh and Rician fading channel conditions. The mean square tracking error or the variance of the normalized tracking error was plotted against the SNR.

The non-coherent DLL analyzed in Chapter 3 was digital. Consequently, the Fokker-Plank method could not be applied to obtain the PDF for this loop. The loop tracking error was modeled by a discrete time first-order Markov process. The transition probability of this Markov process was obtained in closed form. The system model took into account multipath interference and quadrature phase spreading. The PDF of the normalized tracking error for the non-coherent DLL was obtained by using the transition and initial error PDFs and by iterating the Kolmogorov-Chapman equation for the tracking error process. It was seen that the RAKE-like combining DLL also outperforms the NC-DLL at all values of SNR. Even for SNR values as large as 10 dB, there still exists an irreducible performance floor for the traditional NC-DLL. Our results show that under Rician fading, the performance of both the DLLs (combining and non-coherent) is improved as compared to that under Rayleigh fading.

Multiple access interference was considered in Chapter 4, where the previous performance analysis was used to obtain time-of-arrival estimation accuracy for positioning scenarios in CDMA networks. Three different scenarios were considered on the basis of the geometry of the MS and its co-locating BSs: no handoff (Case 1), 2-way handoff (Case 2) and 3-way handoff (Case 3). In all these cases, the non-coherent DLL was considered, as it is the mostly widely used in practice. It was seen that DLL performance improves as the number of hand-offs increase. The tracking error PDFs for line-of-sight and non-line-of-sight signal propagation were compared. LOS conditions offer better performance than NLOS conditions. It was also seen that the mean square tracking error increases linearly with the number of users in a cell.

5.2 Recommendations for Future Work

In this work, the multipath interference was modeled by using two uncorrelated paths. Furthermore, the delay of each path was fixed. Consideration of more comprehensive multipath channel models can be addressed in future work. This might include three or more *correlated* multipaths with random individual delays. Also, a slowly time-varying channel was assumed or equivalently a static MS and static surrounding environment were modeled. Future investigations could consider fast fading, where either MS is moving or its surrounding environment is changing fast relative to the chip duration of the CDMA signal.

This work analyzes only the ToA measurements taken from DLLs. As discussed in Chapter 1, other methods are also available for ToA measurements. They include frequency-domain algorithms, subspace-based code acquisition and Kalman filtering on the incoming CDMA signal. Future work can analyze and compare the measurements based on these methods.

The analysis done in the present study can also be extended to analyze other system parameters for the CDMA receiver such as bit/symbol error probabilities. In analyzing error probabilities, perfect code synchronization is usually assumed between the receiver and the transmitter. Given the statistics of the timing error for the code tracking loop, a more realistic model for the CDMA receiver can be considered and hence error probabilities can be computed more accurately.

Appendix A

A.1 First-Order Markov Processes and the One-Dimensional Fokker-Plank Equation

The one-dimensional Fokker-Plank equation corresponding to a Markov process is derived. Such a process is described by the stochastic differential equation developed for the RAKE-like combining DLL given in chapter 2. For a Markovian process the marginal PDF $p(x_1, t_1)$ and the transition p.d.f. $p(x_1, t_1|x_2, t_2)$ are related to the marginal PDF $p(x_2, t_2)$ through

$$p(x_1, t_1) = \int_{-\infty}^{\infty} p(x_1, t_1|x_2, t_2)p(x_2, t_2)dx_2 \tag{A.1}$$

where we have used the notation $p(x_2, t_2) \triangleq p[x(t_2)]$ and $p(x_1, t_1|x_2, t_2) \triangleq p[x(t_1)|x(t_2)]$ in order that the time origin be kept definite with respect to the dummy variables x_1 and x_2.

Consider the conditional characteristic function of the *random increment* $\Delta x = x_1 - x_2$ given by

$$C_{\Delta x}(\omega) = \int_{-\infty}^{\infty} e^{i\omega(x_1 - x_2)} p(x_1, t_1|x_2, t_2)dx_1 \tag{A.2}$$

which occurs during the time interval (t_1, t_2) given that $x(t_2) = x_2$. The inverse Fourier transform gives

$$p(x_1, t_1|x_2, t_2) = \frac{1}{2\pi} \int_{-\infty}^{\infty} e^{-i\omega(x_1 - x_2)} C_{\Delta x}(\omega)d\omega \tag{A.3}$$

Substituting A.3 into A.1 gives

$$p(x_1, t_1) = \frac{1}{2\pi}\int_{-\infty}^{\infty} p(x_2, t_2) \int_{-\infty}^{\infty} e^{-i\omega(x_1 - x_2)} C_{\Delta x}(\omega)\, d\omega\, dx_2 \tag{A.4}$$

Using the definition of the characteristic function $C_{\Delta x}(\omega)$ as a power-series with moments as the coefficients of terms gives

$$\begin{aligned} C_{\Delta x}(\omega) &= \sum_{q=0}^{\infty} \frac{(i\omega)^q}{q!} E[(\Delta x)^q] \\ &= \sum_{q=0}^{\infty} \frac{(i\omega)^q}{q!} E[(x_1 - x_2)^q] \\ &= \sum_{q=0}^{\infty} \frac{(i\omega)^q}{q!} m_q(\Delta x) \end{aligned} \tag{A.5}$$

where $m_q(\Delta x)$ is the q^{th} moment function of the random increment $x_1 - x_2$. It follows that

$$p(x_1, t_1) = \frac{1}{2\pi}\sum_{q=0}^{\infty} \frac{1}{q!} \int_{-\infty}^{\infty} p(x_2, t_2) \int_{-\infty}^{\infty} m_q(\Delta x) e^{-i\omega(x_1 - x_2)} (i\omega)^q\, d\omega\, dx_2 \tag{A.6}$$

But

$$\begin{aligned} \frac{1}{2\pi}\int_{-\infty}^{\infty} e^{-i\omega(x_1 - x_2)} (i\omega)^q\, d\omega &= \frac{1}{2\pi}\left(-\frac{\partial}{\partial x_1}\right)^q \int_{-\infty}^{\infty} e^{-i\omega(x_1 - x_2)} d\omega \\ &= \left(-\frac{\partial}{\partial x_1}\right)^q \delta(x_1 - x_2) \end{aligned} \tag{A.7}$$

so that A.6 becomes

$$p(x_1,t_1) = \sum_{q=0}^{\infty} \frac{1}{q!} \int_{-\infty}^{\infty} p(x_2,t_2)\, m_q(\Delta x) \left(-\frac{\partial}{\partial x_1}\right)^q \delta(x_1 - x_2)\, dx_2$$
$$= p(x_1,t_2) + \sum_{q=0}^{\infty} \frac{1}{q!} \left(-\frac{\partial}{\partial x_1}\right)^q m_q(\Delta x)\, p(x_1,t_2) \tag{A.8}$$

If $p(x_1,t_1) = p(x_1,t_2) = p_s(x_1,t)$ for all t, then the process is *stationary* of order one and A.8 reduces to

$$\sum_{q=0}^{\infty} \frac{1}{q!} \left(-\frac{\partial}{\partial x_1}\right)^q m_q(\Delta x)\, p_s(x_1,t) = 0 \tag{A.9}$$

Returning to A.8 and setting $t_2 = t$, $t_1 = t + \tau$, $x_2 = x$, $x_1 = x_\tau$ we can write

$$p(x_\tau, t+\tau) - p(x_\tau, t) = \sum_{q=0}^{\infty} \frac{1}{q!} \left(-\frac{\partial}{\partial x_1}\right)^q E[(x_\tau - x)^q]\, p(x,t) \tag{A.10}$$

Dividing by τ and passing to the limit $\tau \to 0$, we obtain

$$\frac{\partial p(x,t)}{\partial t} = \sum_{q=0}^{\infty} \frac{1}{q!} \left(-\frac{\partial}{\partial x}\right)^q k_q(x)\, p(x,t) \tag{A.11}$$

where

$$k_q(x) = \lim_{\tau \to 0} \frac{E[(x_\tau - x)^q]}{\tau} \tag{A.12}$$

provided that the limit exists. If the intensity coefficients $k_q = 0, q \geq 3$, then A.11 becomes the well-known one-dimensional Fokker-Plank equation; that is

$$\frac{\partial}{\partial x}[k_1(x)p(x,t)] - \frac{1}{2}\frac{\partial^2}{\partial x^2}[k_2(x)p(x,t)] + \frac{\partial p(x,t)}{\partial t} = 0 \tag{A.13}$$

A.2 Steady State Solution of the Fokker-Plank equation

We recast A.13 as follows:

$$\boldsymbol{\nabla} \cdot \mathcal{J}(x,t) + \frac{\partial p(x,t)}{\partial t} = 0 \tag{A.14}$$

where we have introduced the probability current flowing in the positive direction of the x axis

$$\mathcal{J}(x,t) \triangleq \left[k_1(x) - \frac{1}{2}\frac{\partial}{\partial x}k_2(x)\right]p(x,t) \tag{A.15}$$

and $\boldsymbol{\nabla} = \partial/\partial t$ In the steady state $\boldsymbol{\nabla} \cdot \mathcal{J} = 0$, equation A.14 becomes a linear differential equation in $p(x)$,

$$\frac{d}{dx}[k_2(x)p(x)] - 2k_1(x)p(x) = -2\mathcal{J} \tag{A.16}$$

The general solution to A.16 can be obtained by introducing the change of variables $v(x) = k_2(x)p(x)$ to yield

$$\frac{dv}{dx} - h(x)v(x) = -2\mathcal{J} \tag{A.17}$$

where we have introduced the restoring force, relative to $k_2(x)$,

$$h(x) = \frac{2k_1(x)}{k_2(x)} = -\nabla u(x) \tag{A.18}$$

and the potential function

$$u(x) = -\int^{x} h(y)\, dy = -\int^{x} \frac{2k_1(x)}{k_2(x)}\, dy \tag{A.19}$$

Multiplying both sides of A.17 by the integrating factor $\exp[u(x)]$, we can write

$$\frac{d}{dx}\{v(x)e^{u(x)}\}u(x) = -2\mathcal{J}e^{u(x)} \tag{A.20}$$

When we integrate with respect to x and multiply the result by $e^{-u(x)}$, A.20 becomes

$$v(x) = e^{-u(x)}\left[C - 2\mathcal{J}\int^{x} e^{u(y)}\, dy\right] \tag{A.21}$$

which says that

$$p(x) = \frac{e^{-u(x)}}{k_2(x)}\left[C - 2\mathcal{J}\int^{x} e^{u(y)}\, dy\right] \tag{A.22}$$

Appendix B

B.1 Calculation of k_2 in Equation 2.28

$$\begin{aligned} k_2 &= k_L^2 \int_{-\infty}^{\infty} R_{n_T}(\xi) d\xi \\ &= k_L^2 \int_{-\infty}^{\infty} E[n_T(t) n_T(t+\xi)] d\xi \end{aligned} \tag{B.1}$$

To compute k_2 we first calculate $R_{n_T}(\xi)$,

$$\begin{aligned} R_{n_T}(\xi) &= E[n_T(t) n_T(t+\xi)] \\ &= E\left[\left(\frac{1}{\sqrt{2}}\sum_{k=0}^{L} a_k \left(w_{Ik}(t) + w_{Qk}(t)\right)\right)\left(\frac{1}{\sqrt{2}}\sum_{j=0}^{L} a_j \left(w_{Ij}(t+\xi) + w_{Qj}(t+\xi)\right)\right)\right] \\ &= \frac{1}{2}\sum_{k=0}^{L}\sum_{j=0}^{L} a_j a_k \big(E\big[w_{Ik}(t) w_{Ij}(t+\xi)\big] + E\big[w_{Ik}(t) w_{Qj}(t+\xi)\big] \\ &\qquad + E\big[w_{Qk}(t) w_{Ij}(t+\xi)\big] + E\big[w_{Qk}(t) w_{Qj}(t+\xi)\big]\big) \\ &= \frac{1}{2}\sum_{k=0}^{L}\sum_{j=0}^{L} a_j a_k \big(R_{II}^{kj}(\xi) + R_{IQ}^{kj}(\xi) + R_{QI}^{kj}(\xi) + R_{QQ}^{kj}(\xi)\big) \end{aligned} \tag{B.2}$$

In computing the individual correlations in 2.41, the following fact is useful:

$$\left.\begin{aligned} y_1(t) &= h(t) * x_1(t) \\ y_2(t) &= h(t) * x_2(t) \end{aligned}\right\} \Rightarrow R_{y_1y_2}(\xi) = E[y_1(t)y_2(t+\xi)]$$

$$= R_{x_1x_2}(\xi) * h(-\xi) * h(\xi) \tag{B.3}$$

$$= E[x_1(t)x_2(t+\xi)] * h(-\xi) * h(\xi)$$

The above fact is applied to compute $R_{II}^{kj}(\xi)$ (with $R_{II}^{kj}(\xi) = E\left[w_{Ik}(t)w_{Ij}(t+\xi)\right]$).

First, setting $y_1(t)$ and $y_2(t+\xi)$ to the expressions for $w_{Ik}(t)$ and $w_{Ij}(t+\xi)$ we get

$$\begin{aligned} y_1(t) &= w_{Ik}(t) \\ &= n_{Ik}^c(t)\cos(\theta_k) + n_{Ik}^s(t)\sin(\theta_k) \\ &= n_c(t)c_{I\Delta}(t-\hat{\tau}-kT_c)\cos(\theta_k) * \tilde{h}(t) + n_s(t)c_{I\Delta}(t-\hat{\tau}-kT_c)\sin(\theta_k) * \tilde{h}(t) \\ &= \{n_c(t)c_{I\Delta}(t-\hat{\tau}-kT_c)\cos(\theta_k) + n_s(t)c_{I\Delta}(t-\hat{\tau}-kT_c)\sin(\theta_k)\} * \tilde{h}(t) \end{aligned} \tag{B.4}$$

$$\begin{aligned} y_2(t+\xi) &= w_{Ij}(t+\xi) \\ &= n_{Ij}^c(t+\xi)\cos(\theta_k) + n_{Ij}^s(t+\xi)\sin(\theta_k) \\ &= n_c(t+\xi)c_{I\Delta}(t+\xi-\hat{\tau}-jT_c)\cos(\theta_k) * \tilde{h}(t+\xi) \\ &\quad + n_s(t+\xi)c_{I\Delta}(t+\xi-\hat{\tau}-jT_c)\sin(\theta_k) * \tilde{h}(t+\xi) \\ &= \{n_c(t+\xi)c_{I\Delta}(t-\hat{\tau}-jT_c)\cos(\theta_j) \\ &\quad + n_s(t+\xi)c_{I\Delta}(t+\xi-\hat{\tau}-jT_c)\sin(\theta_j)\} * \tilde{h}(t+\xi) \end{aligned} \tag{B.5}$$

Hence,

$$
\begin{aligned}
R_{II}^{kj}(\xi) &= E\left[w_{Ik}(t)w_{Ij}(t+\xi)\right] \\
&= E\Big[(n_c(t)c_{I\Delta}(t-\hat{\tau}-kT_c)\cos(\theta_k) \\
&\qquad + n_s(t)c_{I\Delta}(t-\hat{\tau}-kT_c)\sin(\theta_k))\big(n_c(t+\xi)c_{I\Delta}(t+\xi-\hat{\tau}-jT_c) \\
&\qquad \times \cos\big(\theta_j\big) + n_s(t+\xi)c_{I\Delta}(t+\xi-\hat{\tau}-jT_c)\sin\big(\theta_j\big)\big)\Big] * \tilde{h}(-\xi) * \tilde{h}(\xi) \\
&= \{\underbrace{E[n_c(t)n_c(t+\xi)]}_{=\frac{N_0}{2}\delta(\xi)} E[c_{I\Delta}(t-\hat{\tau}-kT_c)c_{I\Delta}(t+\xi-\hat{\tau}-jT_c)]\cos(\theta_k)\cos\big(\theta_j\big) \\
&\qquad + \underbrace{E[n_c(t)n_s(t+\xi)]}_{=0} E[c_{I\Delta}(t-\hat{\tau}-kT_c)c_{I\Delta}(t+\xi-\hat{\tau}-jT_c)] \\
&\qquad \times \cos(\theta_k)\sin\big(\theta_j\big) \\
&\qquad + \underbrace{E[n_s(t)n_c(t+\xi)]}_{=0} E[c_{I\Delta}(t-\hat{\tau}-kT_c)c_{I\Delta}(t+\xi-\hat{\tau}-jT_c)] \\
&\qquad \times \sin(\theta_k)\cos\big(\theta_j\big) \\
&\qquad + \underbrace{E[n_s(t)n_s(t+\xi)]}_{=\frac{N_0}{2}\delta(\xi)} E[c_{I\Delta}(t-\hat{\tau}-kT_c) \\
&\qquad \times c_{I\Delta}(t+\xi-\hat{\tau}-jT_c)]\sin(\theta_k)\sin\big(\theta_j\big)\} * \tilde{h}(-\xi) * \tilde{h}(\xi)
\end{aligned}
\tag{B.6}
$$

Assuming that the channel is slowly time varying, the constants θ_k are independent of time. Working out the expectations in 2.45, the expression for $R_{II}^{kj}(\xi)$ is

$$R_{II}^{kj}(\xi) = \frac{N_0}{2}\delta(\xi)\cos(\theta_k - \theta_j)\left\{2R_I\left(\frac{\xi}{T_C} + k - j\right)\right.$$
$$\left. - R_I\left(\frac{\xi}{T_C} + k - j + 2\Delta\right) - R_I\left(\frac{\xi}{T_C} + k - j - 2\Delta\right)\right\} * \tilde{h}(-\xi) * \tilde{h}(\xi)$$
$$= \frac{N_0}{2}\cos(\theta_k - \theta_j)\{2R_I(k - j)$$
$$- R_I(k - j + 2\Delta) - R_I(k - j - 2\Delta)\}\int_{-\infty}^{\infty}\left|\tilde{H}(f)\right|^2 e^{-j2\pi f\xi}df \quad \text{(B.7)}$$

The expression for $R_{QQ}^{kj}(\xi)$ is the same as above. Also $R_{IQ}^{kj}(\xi) = R_{QI}^{kj}(\xi) = 0$, under the assumption that I and Q code sequences are orthogonal to each other.

Using the definition of k_2 in 2.37,

$$
\begin{aligned}
k_2 &= k_L^2 \int_{-\infty}^{\infty} R_{n_T}(\xi) d\xi \\
&= k_L^2 \int_{-\infty}^{\infty} \frac{1}{2} \sum_{k=0}^{L} \sum_{j=0}^{L} a_j a_k \left(R_{II}^{kj}(\xi) + R_{QQ}^{kj}(\xi) \right) \\
&= k_L^2 \int_{-\infty}^{\infty} \sum_{k=0}^{L} \sum_{j=0}^{L} a_j a_k R_{II}^{kj}(\xi) \\
&= k_L^2 \frac{N_0}{2} \Bigg\{ [1 - R_I(2\Delta)] \sum_{k=0}^{L} a_k^2 \\
&\qquad - R_I(1 - 2\Delta) \sum_{k=0}^{L-1} a_k a_{k+1} \cos(\theta_k - \theta_{k+1}) \\
&\qquad - R_I(2 - 2\Delta) \sum_{k=0}^{L-2} a_k a_{k+2} \cos(\theta_k - \theta_{k+2}) \Bigg\} \\
&\qquad \cdot \int_{-\infty}^{\infty} \int_{-\infty}^{\infty} \left| \widetilde{H}(f) \right|^2 e^{-j2\pi f \xi} df d\xi
\end{aligned}
\tag{B.8}
$$

Working out the integral in 2.47 gives

$$
\begin{aligned}
k_2 = \frac{k_L^2 \left| \widetilde{H}(0) \right|^2 N_0}{2} \Bigg\{ & [1 - R_I(2\Delta)] \sum_{k=0}^{L} a_k^2 \\
& - R_I(1 - 2\Delta) \sum_{k=0}^{L-1} a_k a_{k+1} \cos(\theta_k - \theta_{k+1}) \\
& - R_I(2 - 2\Delta) \sum_{k=0}^{L-2} a_k a_{k+2} \cos(\theta_k - \theta_{k+2}) \Bigg\}
\end{aligned}
\tag{B.9}
$$

Bibliography

[1] T. S. Rappaport, *Wireless Communications Princpels and Practice.*: Pearson Education Inc., 2002.

[2] J. G. Proakis, *Digital Communications*, 4th ed.: McGraw-Hill Education, 2000.

[3] S. Glisic and B. Vucetic, *Spread Spectrum CDMA Systems for Wireless Communications.*: Artech House Mobile Communication Series, 1997.

[4] M. K. Simon, J. K. Omura, R. A. Scholtz, and B. K. Levitt, *Spread Spectrum Communications Handbook.*: McGraw Hill Inc., 1994.

[5] R. E. Ziemer, R. L. Peterson, and D. E. Borth, *Introduction to Spread Spectrum Communications.*: Prentice Hall, 1995.

[6] J. J. Spilker and D. T. Magill, "The Delay-Lock Discriminator--An Optimum Tracking Device," *Proc. IRE*, vol. 49, pp. 1403-1416, 1961.

[7] J. J. Spilker, "Delay Lock Tracking of Binary Signals," *IEEE Trans. on Space Electron Telem.*, vol. SET-9, pp. 1-8, 1963.

[8] W. J. Gill, "A Comparison of Binary Delay Lock Loop Implementations," *IEEE Trans. on Aerospace Electronic Systems*, vol. AES-2, pp. 415-424, 1966.

[9] M. Simon, "Noncoherent Pseudonoise Code Tracking Performance of Spread Spectrum Receivers," *IEEE Trans. on Communications*, vol. 25, pp. 327-345, 1977.

[10] M. Feuerstein and A. Pratt, "A Local Area Positioning System," in *Fifth International Conference on Mobile Radio and Personal Communications*, 1989, pp. 79-83.

[11] W. Figel, N. Sheperd, and W. Trammell, "Vehicle Location by a Signal Attenuation Method," *IEEE Trans. on Vehicular Technology*, vol. VT-18, pp. 105-110, November 1969.

[12] M. Gans, "A Power Spectral Theory of Propagation in Mobile-Radio Environment," *IEEE Trans. on Vehicular Technology*, vol. 21, pp. 27-38, February 1972.

[13] H. Hashemi, "Pulse Ranging Radiolocation Technique on Its Application to Channel Assignment in Digital Cellular Radio," in *IEEE Vehicular Technology Conference*, 1991, pp. 675-680.

[14] M. Hata and T. Nagatsu, "Mobile Location Using Signal Strength Measurements in a Cellular System," *IEEE Trans. on Vehicular Technology*, vol. VT-29, pp. 245-251, May 1980.

[15] G. Ott, "Vehicle Location in Cellular Mobile Radio Systems," *IEEE Trans. on Vechicular Technology*, vol. VT-26, pp. 43-46, February 1977.

[16] S. Sakagami and et. Al, "Vehicle Position Estimates by Mulitbeam Antennas in Multipath Environments," *IEEE Trans on Vehicular Technology*, vol. 41, pp. 63-67, February 1992.

[17] H. L. Song, "Automatic Vehicle Location in Cellular Communication Systems," *IEEE Trans. on Vehcular Technology*, vol. 43, pp. 902-908, November 1994.

[18] J. J. Caffery, *Wireless Location in CDMA Cellular Radio Ssytem*. Massachusetts: Kluwer Academic Publishers, 2000.

[19] J. J. Caffery and G. L. Stuber, "Subscriber Location in CDMA Cellular Networks," *IEEE Trans. on Vehicular Technology*, vol. 47, pp. 406-416, May 1998.

[20] M. Silventoninen and T. Rantalainen, "Mobile Station Emergency Locating in GSM," in *IEEE Int. Conf. on Personal and Wireless Communications*, 1996, pp. 232-238.

[21] R. Lupas and S. Verdu, "Near-Far Resistance of Multiuser Detectors in Asynchronous Channels," *IEEE Trans. on Communciations*, vol. 39, pp. 496-508, April 1990.

[22] J. Holtzman, S. Nanda, and D. Goodman, "CDMA Power Control for Wireless Networks," in *Third Generation of Wireless Information Networks*.: Kluwer Academic Publishers, 1992, pp. 299-311.

[23] W. Lee, "Power Control in CDMA," in *IEEE Vehicular Technology Conference*, 1991, pp. 77-80.

[24] J. J. Caffery and G. L. Stuber, "Radio Location in Urban CDMA Microcells," in *IEEE Personal Indoor Mobile Radio Conference*, 1994, pp. 1227-1231.

[25] P. Goud, A. Sesay, and M. Fattouche, "A Spread Spectrum Radiolocation Technique and Its Application to Cellular Radio," in *IEEE Pacific Rim Conference on Communications, Copmuters and Signal Processing*, 1991, pp. 661-664.

[26] K. Kosbar and J. Zaninovich, "Periodic PN Sequence Delay Estimation using Phase Spectrum Data," in *IEEE Global Telecommunications Conference*, 1993, pp. 1665-1669.

[27] M. Pallas and G. Jourdain, "Active Higher Resolution Time Delay Estimation for Large BT Signals," *IEEE Trans. on Signals Processing*, pp. 781-787, April 1991.

[28] H. P. Hartmann, "Analysis of a Dithering Loop for PN Code Tracking," *IEEE Trans. on Aerospace Electronic Syst.*, vol. AES-10, pp. 2-9, 1974.

[29] H. Meyr, "Nonlinear Analysis of Correlative Tracking Systems Using Renewal Process Theory," *IEEE Trans. on Communciations*, vol. 23, pp. 192-203, 1975.

[30] H. Meyr, "Delay-Lock Tracking of Stochastic Signals," *IEEE Trans. on Communications*, vol. 24, pp. 331-339, 1976.

[31] W. Lindsey and H. Meyr, "Complete statistical description of the phase-error process generated by correlative tracking systems," *IEEE Trans. on Information Theory*, vol. 23, pp. 194-202, 1977.

[32] R. Polydoros and C. Weber, "Analysis and Optimization of Corrrelative Code-Tracking Loops in Spread-Spectrum Systems," *IEEE Trans. on Communciations*, pp. 30-43, 1985.

[33] R. Yost and R. Boyd, "A Modified PN Code Tracking Loop: Its Performance Analysis and Comparative Evaluation," *IEEE Trans. on Communciations*, vol. 30, pp. 1027-1036, 1982.

[34] U. P Bernhard, "Influence of data modulation and Doppler effects on the performance of a delay lock loop," in *Spread Spectrum Techniques and Applications, 1994. IEEE ISSSTA '94, Third International Symposium*, 1994.

[35] K. Jamaleddine, D. Vizieranu, F. Malassenet, and S. Halunga, "A new delay locked loop structure with enahnced tracking behavior," in *Seventh IEEE International Symposium on*

Personal, Indoor and Mobile Radio Communications, PIMRC'96, 1996.

[36] S. L. Su and N. Y. Yen, "Performance of Digital Code Tracking Loops for Direct Sequence Spread-Spectrum Signals in Mobile Radio Channels," *IEEE Trans. on Communications*, vol. 45, pp. 596-604, May 1997.

[37] J. J. Caffery and G. L. Stuber, "Effects of Mulitple Access Interference on the Noncoherent Delay Lock Loop," *IEEE Trans. on Communications*, vol. 48, pp. 2109-2119, December 2000.

[38] S. L. Su and N. Y. Yen, "Performance of Combined DDLL and AGC Loop for Direct-Sequence Spread Spectrum Systems," *IEEE Trans. on Communications*, vol. 48, pp. 1455-1458, September 2000.

[39] W. H. Sheen and G. L. Stuber, "Effects of Mulitpath Fading on Delay-Locked Loops for Spread Spectrum Systems," *IEEE Trans. on Communications*, vol. 42, pp. 1947-1956, April 1994.

[40] W. H. Sheen and C. H. Tai, "A Noncoherent Tracking Loop with Diversity and Multipath Interference Cancellation for Direct-Sequence Spread-Spectrum Systems," *IEEE Trans. on Communications*, vol. 46, pp. 1516-1523, November 1998.

[41] W. H. Sheen, M. J. Chang, and C. S. Wu, "Performance analysis of Noncoherent Dgitial Delay Locked Loops for Direct Sequence Spread Systems with Doppler Shift and Quantized Adaptation," *IEEE Trans. on Wireless Communications*, vol. 3, pp. 2108-2111, November 2004.

[42] G. Fock, J. Baltersee, P. Schultze-Rittich, and H. Meyr, "Channel Tracking for Rake Receivers in Closely Spaced Multipath Enivronments," *IEEE Journal on Selected Areas in Communications*, vol. 19, pp. 2420-2430, December 2001.

[43] R. De Gadenzi and M. Luise, "Decision-Directed Coherent Delay-Lock Tracking Loops for DS Spread Spectrum," *IEEE Trans. on Communications*, vol. 39, pp. 758-766, May 1991.

[44] W. H. Sheen and G. L. Stuber, "A New Tracking Loop for Direct Sequence Spread Specturm Systems on Frequency-Selective Fading Channels," *IEEE Trans. on Communications*, vol. 43, pp. 3063-3073, December 1995.

[45] W. C. Lindsey, *Synchronization Systems in Communication and Control*. Englewood Cliffs,

New Jersey: Prentice Hall, 1972.

[46] H. R. Park, "Performance Analysis of a Decision-Feedback Coherent Code Tracking Loop for Pilot-Symbol-Aided DS/SS Systems," *IEEE Trans. on Vehicular Technology*, vol. 55, no. 4, pp. 1249-1258, July 2006.

[47] J. Viterbi, *Principles of Spread Spectrum Communciation.*: Addison-Wesley, 1996.

[48] H. J. Larson and B. O. Shubert, *Probablistic Models in Engineering Sciences, vol II, Random Noise, Signals and Dynamic Systems.*: Prentice Hall, 1985.

[49] M. A. Landolsi, A. H. Muqaibel, and A. S. Al-Ahmari, "Near-Far Problem Impact on Mobile Radiolocation Accuracy in CDMA Wireless Cellular Networks," in *IEEE International Conference on Telecommunication*, 2007.

[50] M. A. Landolsi, A. S. Al-Ahmari, and A. H. Muqaibel, "Development of Robust Technques to Aid Mobile Phone Location in Wireless CDMA Networks," King Abdul Aziz City of Science & Technology (KACST), GDRP Grant #24-87, September 2005-December 2007.